Journal of Colloid and Interface Science 684 (2025) 105–121

Contents lists available at ScienceDirect

Journal of Colloid And Interface Science

journal homepage: www.elsevier.com/locate/jcis

Biliquid oil-in-water nanofoams and spontaneous emulsification obtained with a surfactant resistant to curvature changes

Patrick Denk [a], Selina Reigl [a], Bastian Rödig [a], Michael Sztucki [b], Sylvain Prévost [c], Thomas Zemb [d], Werner Kunz [a,*]

[a] Institute of Physical and Theoretical Chemistry, University of Regensburg D-93053 Regensburg, Germany
[b] European Synchrotron Radiation Facility – The European Synchrotron, 71 avenue des Martyrs F-38043 Grenoble, France
[c] Institut Laue-Langevin – The European Neutron Source, 71 Avenue des Martyrs, CS40220 F-38042 Grenoble Cedex 9, France
[d] Institut de Chimie Séparative de Marcoule, BP 17171 F-30207 Bagnols-sur-Cèze, France

HIGHLIGHTS

- We studied a ternary system water – surfactant – oil with a surfactant that is not able to change curvature completely.
- Instead of a bicontinuous microemulsion, a thermodynamically stable oil-in-water biliquid nanofoam is formed.
- Such an oil-in-water biliquid nanofoam was detected for the first time.
- This nanofoam may be used as a multitude of nanocontainers, e.g., for chemical reactions in a pseudo-aqueous environment.
- We also detected an "Onuki-like" monophasic mesoscopic turbid region in this phase diagram.

GRAPHICAL ABSTRACT

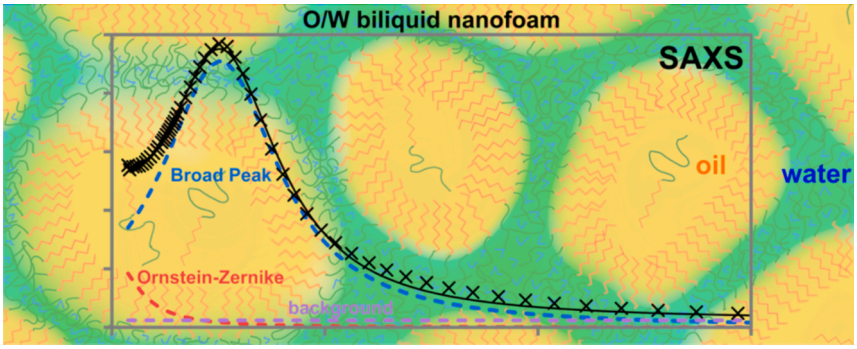

ARTICLE INFO

Keywords:
Nanofoam
Biliquid foam
Emulsification
Microemulsion
Small-angle scattering
Akypo LF2
Alkyl ether carboxylate
Nanoreactors

ABSTRACT

Hypothesis: Due to its huge polar headgroup, octaoxyethylene octyl ether carboxylic acid ($C_8E_8CH_2COOH$ = Akypo LF2™) is supposed not to be able to change its curvature sufficiently to form bicontinuous microemulsions. Instead, upon adding an oil to the binary water – surfactant system, excess oil could be squeezed out or a biliquid foam could form.
Experiments: An auto-dilution setup was used to record small-angle X-ray scattering data along six dilution lines in the newly established phase diagram of the ternary system 2-ethylhexanol – $C_8E_8CH_2COOH$ – water.
Results: Evaluation of the data in combination with the recorded phase diagram revealed that the ternary microemulsions with a slightly amphiphilic oil indeed do not show a classical structural inversion via a bicontinuous structure with increasing oil content, but instead the sequence: O/W micelles – O/W biliquid nanofoam – molecular co-solubilization in the oil phase. The biliquid nanofoam structure with 10^2–10^4 oil molecules enclosed by locally flat layers of interdigitated hydrated headgroups exists in the middle of the phase diagram. We may speculate that this phase can be used as a multitude of nanocontainers, e.g., for chemical reactions in an aqueous environment, but with negligible water chemical potential. In the vicinity of the critical point,

* Corresponding author.
E-mail address: werner.kunz@ur.de (W. Kunz).

https://doi.org/10.1016/j.jcis.2025.01.090
Received 9 December 2024; Received in revised form 7 January 2025; Accepted 11 January 2025
Available online 13 January 2025

spontaneous formation of stable mesoscale droplets (an “Onuki-like” structure, as known with antagonistic salts) is detected in a region showing a pronounced Tyndall effect.

1. Introduction

We have shown in previous studies [1,2] that the binary system octaoxyethylene octyl ether carboxylic acid ($C_8E_8CH_2COOH$) – water has very specific properties. No liquid crystalline phases are formed, and only spherical micelles are found throughout the entire binary phase diagram. Classical core–shell micelles in an aqueous bulk medium (L_1 phase) are formed at high water contents and direct spherical micelles with interdigitated headgroups are formed at low water contents (L_1' phase). The latter can be viewed as a dispersion of hydrocarbon cores in a medium of interdigitated hydrated headgroups. This means that direct micelles without external bulk water exist above 60 wt% of surfactant, where the hydrated headgroups, not the alkyl chains, interdigitate. These observations are a consequence of the surfactant resisting any shape transition for steric reasons. The molecular volume of the headgroup ($V_{head} = 0.606\ nm^3$) is 2.5 times larger than the molecular volume of the tail ($V_{tail} = 0.243\ nm^3$) and becomes effectively even larger when the ethylene oxide units are hydrated by water molecules. Even when dehydrated by increasing temperature, the area per molecule imposed by the bulky headgroup remains too large for a decrease of the surfactant-film curvature to occur. The only exception in the $C_8E_8CH_2COOH$ – water system is a semi-crystalline lamellar L_β phase at low temperatures and very high surfactant concentrations ($\geq$ 90 wt%), where the area per molecule is significantly reduced by crystallization of the headgroups. The existence of such a lamellar phase with crystalline headgroups and fluid alkyl chains (or the reverse) was predicted by O. Mouritsen [3] in the case of lipids. Instead of only two possible states of the surfactant film, crystalline or fluid, there is the possibility in between two melting points to observe an intermediary state with ordered headgroups and fluid chains named liquid-ordered (L_o), or the reverse.

In ternary systems of oil – $C_8E_8CH_2COOH$ – water, where the oil is purely hydrophobic, e.g., *n*-hexane or *n*-dodecane, there is only a narrow isotropic single-phase domain on the oil-poor side of the phase triangle, while the rest of the phase diagram is covered by a large biphasic domain [4]. This indicates that only a certain amount of oil is incorporated into the micellar cores until a maximum swelling of the micelles is reached, and that any excess oil separates as an oil phase, demonstrating that a structural inversion, or even a shape transition to locally lamellar (bicontinuous) structures, is impossible in these cases. So, we investigate here the system with 2-ethylhexanol, also known as isooctanol, resembling a slightly amphiphilic oil that can act as a co-surfactant. 2-ethylhexanol may also be referred to as a “solvo-surfactant” [5], emphasizing that it combines properties of a hydrophobic solvent and a co-surfactant, though the term is usually used if the volatility of the compound is high [6]. Due to its co-surfactant-like nature, 2-ethylhexanol is expected to weaken the steric packing constraint of the surfactant, making shape transitions possible. As will be shown in this work, one obtains a phase diagram that looks similar to phase diagrams typically found for ternary surfactant or hydrotrope systems forming ultra-flexible microemulsions. A biphasic miscibility gap is observed, no liquid crystalline phases are formed, and a strange region with turbid appearance, which becomes blueish-transparent when adding even more water, is found near the critical point on the oil-rich side of the phase diagram.

The aim of this work is to answer the question: Does a structural inversion from oil-in-water to water-in-oil microemulsions in ternary systems of oil – $C_8E_8CH_2COOH$ – water occur with a surfactant film that cannot revert the curvature for steric reasons, and if not, what are the phenomena linked to the conflicting amount of water and oil associated to a spontaneous packing parameter always close to 1/3?

2. Material and methods

2.1. Materials

The surfactant octaoxyethylene octyl ether carboxylic acid, $C_8E_8CH_2COOH$ ($M \approx 541\ g{\cdot}mol^{-1}$), commercialized under the tradename Akypo® LF2 (90.0 wt% active matter, 0.9 wt% NaCl, 9.1 wt% water) was a generous gift by Kao Chemicals GmbH (Emmerich am Rhein, Germany). The surfactant is a technical product with a broad distribution of the degree of ethoxylation, typically containing small amounts of glycolic acid, formic acid, diglycolic acid, polyethylene glycols, and carboxymethylated polyethylene glycols, as well as a few wt % of nonionic polyoxyethylene alkyl ethers and less than 1.5 wt% of various esters of the type $C_8E_xCH_2COOE_yC_8$, as impurities. Hydrophilic non-surfactant impurities and NaCl were removed by cloud point extraction and water was removed by subsequent vacuum drying, for details the reader is referred to ref. [7]. No differences in the binary aqueous phase behavior between different batches of the surfactant were observed.

It is also important to note that the removal of the ester and nonionic surfactant impurities by ion exchange, see refs. [7,8], only has a marginal effect on the binary aqueous phase behavior of the surfactant. In this work, the surfactant was not further purified by ion exchange.

2-ethyl-1-hexanol (≥99.6 %), also known as 2-ethylhexanol or isooctanol, was purchased from Sigma-Aldrich (St. louis, Missouri, USA). *n*-dodecane (≥95 %) was purchased from Carl Roth (Karlsruhe, Germany). The water used for all experiments had a resistivity > 18 MΩ·cm and was obtained from previously distilled water using a Millipore purification system.

2.2. Phase diagram determination

The ternary phase diagram of the system 2-ethylhexanol – $C_8E_8CH_2COOH$ – water was determined by preparing multiple binary mixtures of $C_8E_8CH_2COOH$ and water or $C_8E_8CH_2COOH$ and 2-ethylhexanol and subsequently adding 2-ethylhexanol or water. During the stepwise addition, the macroscopic appearance of the samples was checked by visual observation and samples were checked for optical anisotropy between crossed polarizers. The temperature was controlled and kept constant at 25 °C using a Julabo (Seelbach, Germany) F32-HD refrigerated and heating circulator. The critical point was determined by letting the samples completely phase separate when reaching the biphasic regime, identifying the sample where both phases are equal in volume. Only two phases were observed in equilibrium, even well inside the biphasic domain.

2.3. Density measurements

Physical densities were measured using a density meter DMA 5000 M from Anton Paar (Graz, Austria), which operates with the oscillating U-tube method. A prerequisite for each measurement was temperature stability with a maximum deviation of ± 0.002 °C.

2.4. Molecular volumes and scattering length densities

Molecular volumes and X-ray scattering length densities (SLDs) of the surfactant, also split into a hydrophobic tail and a hydrophilic headgroup, water (H_2O), and 2-ethylhexanol are given in **Note S1**, which includes details on their calculation.

2.5. Small-angle X-ray scattering

Small-angle X-ray scattering (SAXS) data were recorded on the ID02 [9], TRUSAXS, beamline at the ESRF in Grenoble, France during granted beamtime with the proposal number SC-5453. Samples were measured in a flow-through quartz capillary (inner diameter of 2 mm, 50 µm quartz thickness, Hilgenberg GmbH, Malsfeld, Germany). The detector was an Eiger2 Si 4 M pixel array detector from Dectris (Baden-Daettwil, Switzerland), and the sample transmission was measured simultaneously. 2D SAXS patterns were measured at a sample-to-detector distance of 1 m, covering a total q range of 0.076–7.6 nm^{-1}, where q is the magnitude of the wavevector: $q = 4\pi\cdot\lambda^{-1}\cdot\sin(\theta/2)$, θ being the scattering angle. A fixed wavelength of 0.099 nm was chosen ($\Delta E/E \approx 10^{-4}$). The flow-through capillary was connected to an auto-dilution setup to allow for convenient recording of dilution lines in the phase diagram. The capillary temperature was kept constant at 25 °C using a Peltier stage LFI-3751 from Wavelength Electronics (Bozeman, Montana, USA). However, the whole auto-dilution apparatus was not temperature controlled but exposed to the room temperature slightly below 25 °C. The auto-dilution setup and procedure are described in section 2.5.1. (Fig. 1). An average over 20 scans with an exposure time of 0.1 s per scan provides the standard deviation and corresponding error-bars (not shown in the figures for clarity). An empty capillary was used as a background subtracted from all data files. Data were corrected for flat field, spatial distortion, electronic and dark noise, and transmitted flux. If not stated otherwise, 1D data are radially averaged. 1D data were normalized using the level of water as a standard ($d\sigma/d\Omega$ = 0.0163 cm^{-1}) and dividing by the corresponding path length (2 mm).

2.5.1. Auto-dilution setup

To elucidate the microstructures, SAXS data were recorded at the beamline ID02 [9] along six dilution lines throughout the phase diagram, as indicated in Fig. 2. This was achieved using an auto-dilution setup, schematically depicted in Fig. 1, comprising a mixing chamber with a magnetic stirrer with four in-/outlets, a flow-through 2 mm quartz capillary, one larger peristaltic pump for continuous flow, two smaller peristaltic pumps for controlled addition of a selected component to the system and withdrawal of mixture from the system. To reduce the required amount of material, the dilution was performed at (more or less) constant total volume, i.e., after addition of a certain volume and subsequent mixing, the same volume of mixture was removed from the system.

The following experimental procedure was generally followed:

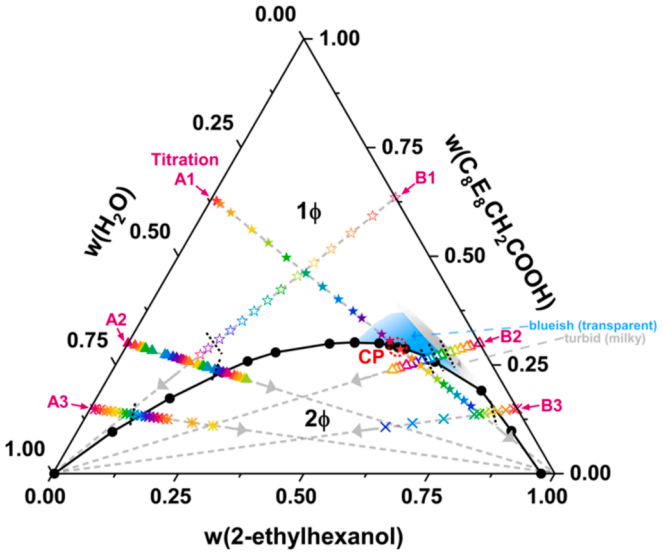

Fig. 2. Phase diagram of the ternary system 2-ethylhexanol – $C_8E_8CH_2COOH$ – H_2O at 25 °C. Points measured by SAXS along six dilution lines (titrations A1, A2, A3, B1, B2, and B3) are indicated as colored symbols. Short black dotted lines indicate the onset of phase transitions observed during the titration. 1ϕ: Monophasic mixture. 2ϕ: Two phases in equilibrium. CP: Critical point.

1. Measurement of the initial composition under continuous flow (20 scans of 0.1 s exposure time each).
2. Addition of a certain volume V (of either H_2O or 2-ethylhexanol) via a peristaltic pump.
3. Equilibration for at least 1 min and subsequent measurement with 20 scans of 0.1 s exposure time each. Mixing was achieved by continuous flow and a magnetic stirrer, and the appearance of the mixture was observed live with a camera.
4. Withdrawal of the volume V with a second peristaltic pump.

… (Repeat steps 2.–4.)

Due to changes in density and viscosity, the actual compositions cannot be calculated from a calibrated pumped volume. Instead, the transmissions were used to calculate the compositions at each measurement in volume fractions using the Beer-Lambert law. To convert the initial sample composition known in weight fractions into volume fractions, ideal mixing, i.e., no volume contraction, was assumed. The

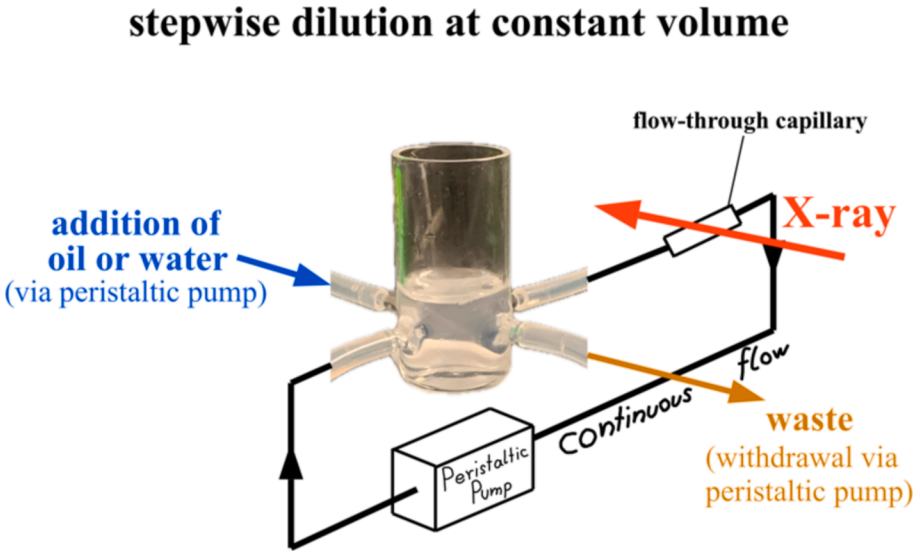

Fig. 1. Schematic drawing of the used auto-dilution setup.

physical densities of the pure components are given in **Note S1**. To convert the volume fractions of the obtained mixtures along the dilution lines back to weight fractions, ideal mixing was assumed likewise. Therefore, it should be noted that the positions of the measured compositions along the dilution lines, as given in Fig. 2, are not exact, but typically the error does not exceed ± 1 wt%. It should also be noted that the first measurement of a given titration, before starting the titration, is not necessarily identical to the initial mixture, as a small amount of the added component can leak out of the respective tube.

The (calculated) compositions of the measured samples during the six titrations, labelled as A1, A2, A3, B1, B2, and B3, are given in Tables S1, S2, S3, S4, S5, and S6, respectively.

2.5.2. Strategy of data evaluation

2.5.2.1. Scattering invariants. The experimental invariant Q, also known as Porod invariant, is given as

$$Q = \int_0^\infty I(q)\cdot q^2 dq \tag{1}$$

and is therefore obtained from the experimental data by integration of $I(q)\cdot q^2$ as a function of q. Before plotting $I(q)\cdot q^2$ as a function of q and calculating the invariant, a flat background, typically equal to the lowest measured intensity, was subtracted from the data. To extrapolate $I(q)\cdot q^2$ to $q = 0$, the simplest approximation of a virtual point at $I(q)\cdot q^2 = 0$ and $q = 0$, i.e., linear approximation between this point and the point measured at the lowest q value, was used. In the case of an increasing scattering intensity at high q values due to molecular scattering, the high-q range above the local minimum was omitted because only the mesoscale structuring is of interest here. Exemplarily for titration A1, the process is graphically depicted in **Fig. S1**.

The experimental invariant is equal to the square of scattering length density (SLD)-weighted spatial fluctuations, known as the theoretical invariant

$$Q_{th} = \pi^2 \sum_{ij} \phi_i \phi_j \Delta SLD_{i|j}{}^2, \tag{2}$$

where ϕ_i is the volume fraction of domain i with the scattering length density SLD_i and $\Delta SLD^2_{i|j} = (SLD_i - SLD_j)^2$ is the contrast between domains i and j. The invariant is independent of shape, size, and size distribution of scatterers and independent of interactions between scatterers, and only requires well-defined domains with sharp interfaces. In the case of two domains, i.e., homogeneous scatterers in a matrix, Q_{th} is given by

$$Q_{th} = 2\pi^2 \phi_1 (1 - \phi_1) \Delta SLD_{1|2}{}^2. \tag{3}$$

In the case of three domains, e.g., two liquid domains separated by a homogeneous film, Q_{th} is given by

$$Q_{th} = 2\pi^2 \left[\phi_1\phi_2 \Delta SLD_{1|2}{}^2 + \phi_2\phi_3 \Delta SLD_{2|3}{}^2 + \phi_3\phi_1 \Delta SLD_{3|1}{}^2\right]. \tag{4}$$

The (monophasic) mixtures in this study consist of at least two domains and a maximum of four domains. Two domains are present for example in the surfactant-rich corner of the phase diagram, where 2-ethylhexanol is incorporated into the surfactant film of the micelles and water is bound to the headgroups as hydration water (L_1' phase). Three domains are found for example in the (swollen) core–shell micellar regime (L_1 phase). Four domains exist, whenever a 2-ethylhexanol-rich pseudo-phase coexists with a water-rich pseudo-phase separated by a surfactant film: 1) A water-rich domain, 2) a 2-ethylhexanol-rich domain, 3) the hydrophilic part of the surfactant film (headgroups + water), and 4) the hydrophobic part of the surfactant film (tails + 2-ethylhexanol). As can be inferred from the SLDs and contrasts given in **Note S1**, the contrast between the hydrophilic part of the surfactant film and 2-ethylhexanol is typically around 1.8 times higher than the contrast between water and 2-ethylhexanol, while the contrast between the hydrophobic part of the surfactant film and water is around 1.2 times larger than the contrast between 2-ethylhexanol and water. Further, the contrast between the hydrophobic part and the hydrophilic part of the surfactant film is typically around 2.1 times larger than the contrast between 2-ethylhexanol and water, meaning that the contribution of the internal contrast of the surfactant film is not negligible. However, the contrast between the hydrophobic part and the hydrophilic part of the surfactant film is typically around 1.7 times higher than the contrast between the hydrophobic part and water, and only around 1.2 times higher than the contrast between the hydrophilic part and 2-ethylhexanol. As the contrast contribution of the hydrophilic part of the surfactant film is dominant over the contribution of its hydrophobic part, in a first approximation one can neglect the hydrophobic part of the surfactant film and consider it as part of the 2-ethylhexanol phase. Then only three instead of four domains need be considered theoretically.

2.5.2.2. Fitting to the Teubner-Strey expression. The Teubner-Strey model [10], described by the following equation and frequently employed for fitting scattering curves of microemulsions, was tested for all scattering curves of monophasic samples.

$$I(q) = scale \cdot \frac{8\cdot\pi\cdot\langle\eta^2\rangle\cdot\frac{c_2}{\xi}}{a_2 + c_1\cdot q^2 + c_2\cdot q^4} + background, \tag{5}$$

where *scale* is a simple scaling factor, typically fixed to $scale = 1$, *background* is a constant "flat" background scattering contribution, $\langle\eta^2\rangle$ is the mean square of the scattering length density fluctuation, and ξ is the correlation length. The parameters a_2, c_1, and c_2 are defined in terms of the correlation length ξ and the periodicity d.

$$a_2 = \left[1 + \left(\frac{2\cdot\pi\cdot\xi}{d}\right)^2\right]^2 \tag{6}$$

$$c_1 = -2\cdot\xi^2\cdot\left(\frac{2\cdot\pi\cdot\xi}{d}\right)^2 + 2\cdot\xi^2 \tag{7}$$

$$c_2 = \xi^4 \tag{8}$$

It is useful to factor out the parameter c_2 in eq. (5) and to define a set of two parameters, a and b, instead of the previous three parameters (a_2, c_1, and c_2), see ref. [11].

$$a^2 = \frac{a_2}{c_2} = \left[\frac{1}{\xi^2} + \left(\frac{2\cdot\pi}{d}\right)^2\right]^2 \tag{9}$$

$$-2\cdot b = \frac{c_1}{c_2} = -2\cdot\left[\left(\frac{2\cdot\pi}{d}\right)^2 - \frac{1}{\xi^2}\right] \tag{10}$$

In the case of a two-(pseudo-)phase system of two (pseudo-)phases A and B with sharp interfaces, $\langle\eta^2\rangle$ is given by

$$\langle\eta^2\rangle = \phi_A\cdot(1 - \phi_A)\cdot(SLD_A - SLD_B)^2. \tag{11}$$

If thermodynamically stable monophasic mixtures are considered, A and B are pseudo-phases. Let A be the polar pseudo-phase and B be the apolar pseudo-phase. If a water-rich pseudo-phase coexists with an oil-rich pseudo-phase, naturally the water-rich pseudo-phase is part of A and the oil-rich pseudo-phase is part of B. In an approximation, the surfactant film in between these two pseudo-phases can be split into the apolar tails as part of B and the polar headgroups as part of A. This approximation is excellent if the SLD of the surfactant tail layer is (almost) equal to the SLD of the oil, in this case 2-ethylhexanol, and if the SLD of the (hydrated) headgroup layer is (almost) equal to the SLD of water, so that there is only one dominant contrast between oil and water. In the present system, see **Note S1**, the (internal) contrast of the

surfactant film is not negligible, i.e., the internal contrast of the surfactant film is typically twice as large as the contrast between water and 2-ethylhexanol. Therefore, the approximation of two pseudo-phases in the Teubner-Strey model is not good in the q range where scattering of the surfactant film is dominant. Thus, typically only the low-q scattering and the peak onset of microemulsion samples in this work are reproduced well. Since the contrast between 2-ethylhexanol and the hydrophobic portion of the surfactant film is very low, the approximation of two pseudo-components holds if A consists only of hydrated headgroups, i.e., if there is no bulk water phase.

The values of SLD_A and SLD_B of course depend on the compositions of the pseudo-phases A and B, including for example the fraction of surfactant dissolved in B (2-ethylhexanol) as an unknown parameter. Because of that, the fits can be used to obtain an estimate of the fraction of surfactant dissolved in the 2-ethylhexanol-rich domain. More detailed information on the used model is given in **Note S2**.

2.5.2.3. Fitting to a weak aggregation Ornstein-Zernike + Lorentzian Broad peak model. A more general model, best suited for all cases of weak aggregation studied until now, was also tested. The scattering is approximated as the sum of an Ornstein-Zernike contribution and a (Lorentzian) Broad Peak contribution [11–13].

$$I(q) = \frac{I_{OZ}(0)}{1 + (\xi_{OZ} \cdot q)^2} + \frac{I_{BP}}{\left[1 + \left(\xi_{BP} \cdot \left(q - q_p\right)\right)^m\right]^n} + background, \tag{12}$$

Where *background* accounts for a flat scattering background. The scattering due to fluctuations of concentrations, i.e., due to fluctuations in electron density, is described by the Ornstein-Zernike equation [14]

$$I_{OZ}(q) = \frac{I_{OZ}(0)}{1 + (\xi_{OZ} \cdot q)^2}, \tag{13}$$

where ξ_{OZ} is the correlation length and $I_{OZ}(0)$ is the scattering intensity at $q = 0$. The Ornstein-Zernike model is purely statistical and applies to fluctuations of concentrations in general, making the determination of its origin a delicate point. In ternary systems with weak aggregation, the Ornstein-Zernike term may result either from the presence of a critical point, or from the polydispersity of the aggregates [13]. The latter is typically observed in surfactant-free microemulsions (SFMEs), also known as ultra-flexible microemulsions (UFMEs) [15]. If the used "oil" is not purely hydrophobic, like alkanes or benzene, but slightly amphiphilic, like for example alcohols, the fluid present in the oil-rich corner of the phase diagram is structured and produces scattering close to a Lorentzian peak. A generalized Lorentzian can be analyzed using a Broad Peak contribution, described by the equation [16]

$$I_{BP}(q) = \frac{I_{BP}}{\left[1 + \left(\xi_{BP} \cdot \left(q - q_p\right)\right)^m\right]^n}, \tag{14}$$

where q_p corresponds to the peak position, I_{BP} is the intensity of the peak, and ξ_{BP} is the correlation length. If the exponents are fixed to $m = 2$ and $n = 1$, as in this work, the equation describes a Lorentzian peak. It is important to note that the two correlation lengths are not the same but differ. The only exception is when $q_P = 0$, in which case the Lorentzian equation is identical to the Ornstein-Zernike equation and the two correlation lengths are physically identical.

Since this model is closer to the five-parameter expression established by Coi and Chen [17], used when three length scales are involved, it yields fits closer to the data than the Teubner-Strey model for microemulsion samples, not only fitting well the low-q part and the peak onset, but the complete scattering, though not exactly reproducing the scattering intensity decline as well. As is to be expected, the model cannot fit well data obtained in a swollen micellar regime, since the interfacial film thickness is more than half of the typical granularity D^* derived from the peak position. For any model, a well-defined peak position, corresponding to a typical distance in real space, can be extracted from the fits. Any predictive theory of packing should be able to predict the peak position as a function of the composition using analytical expressions [18].

3. Results

The phase diagram established at 25 °C of the ternary system 2-ethylhexanol – $C_8E_8CH_2COOH$ – H_2O, including the points measured by SAXS along six dilution lines, is shown in Fig. 2. The variable compositions during the titrations were calculated using the X-ray transmissions (see methods section 2.5.1.). These are obtained in volume fractions, which were transformed to weight fractions assuming absence of density anomalies. The precision is typically better than ± 1 wt%. The phase transitions observed during the titrations are indicated between the two respective points of the titrations by a short, dotted line. These transitions match well the transitions expected from the phase diagram. The only exception is titration B1, where a phase separation was observed that should not exist along this dilution line. Due to a lack of additional data, the exact origin of the experimental error remains unclear, but most likely mixing was inhomogeneous at some point(s) during the titration, and during the process of removing a portion of the mixture after each step of the titration, 2-ethylhexanol was slightly enriched in the sample. This would mean that the titration line of B1 would not be straight (as indicated) but curved towards the biphasic regime. Nevertheless, the deviations from the supposed compositions are still expected to be small enough to leave the conclusions drawn from the scattering data unaltered.

Macroscopically, only one isotropic liquid single-phase region and one biphasic region with two isotropic liquid phases in equilibrium are detected, since the surfactant is fully miscible with water as well as with the oil/solvent used.

A strange phenomenon occurs in the middle of the single-phase region in the oil-rich corner near the critical point: A small turbid domain occurs when water is added to a mixture of 2-ethylhexanol and surfactant. When even more water is added, the turbidity vanishes and the sample appears transparent and slightly blueish, i.e., an initially strong Tyndall effect becomes weaker when adding more water. Despite its turbidity, this domain is thermodynamically monophasic, i.e., there is no macroscopic phase separation. This domain will be called "Onuki region" in this work, as the underlying mechanism was first explained by A. Onuki in the case of antagonistic salts [19,20] and later by Okamoto and Onuki in the case of nonionic hydrophobic solutes [21]. The strong scattering observed is not directly diverging at the critical point but is more reminiscent and may also be linked to a "Widom line" described in near-critical fluids [22]. In this Onuki region, a microemulsion with mesoscale droplets up to several hundreds of nm is formed. A more detailed description of the phenomenon occurring in the Onuki region will be given in section 4.

The SAXS data recorded along the six dilution lines, indicated in Fig. 2, are shown in Fig. 3. Apart from a few exceptions, only spectra of monophasic samples are shown. Before any further data evaluation, a few important conclusions can already be drawn by simply looking at the data presented in Fig. 3. In titrations A1–A3, starting from the binary mixtures of surfactant and water, i.e., from core-shell micelles (L_1 phase) or from slightly headgroup-interdigitated core–shell micelles with mainly hydration water (L_1/L_1' phase), a continuous intensity increase associated to a shift of the scattering pattern towards lower q is observed, indicating swelling of the micelles, whatever the morphology may be. Swelling of micelles with a spontaneous packing parameter close to 1/3 induces free energy related to bending away from the preferred curvature.

Within the dilution lines A1–A3, the scattering intensity increases by three orders of magnitude when 2-ethylhexanol is added. Only growing O/W aggregates are detected. Notably the last two samples of titration A1, i.e., A1-12 and A1-13, exhibit scattering curves that are very similar

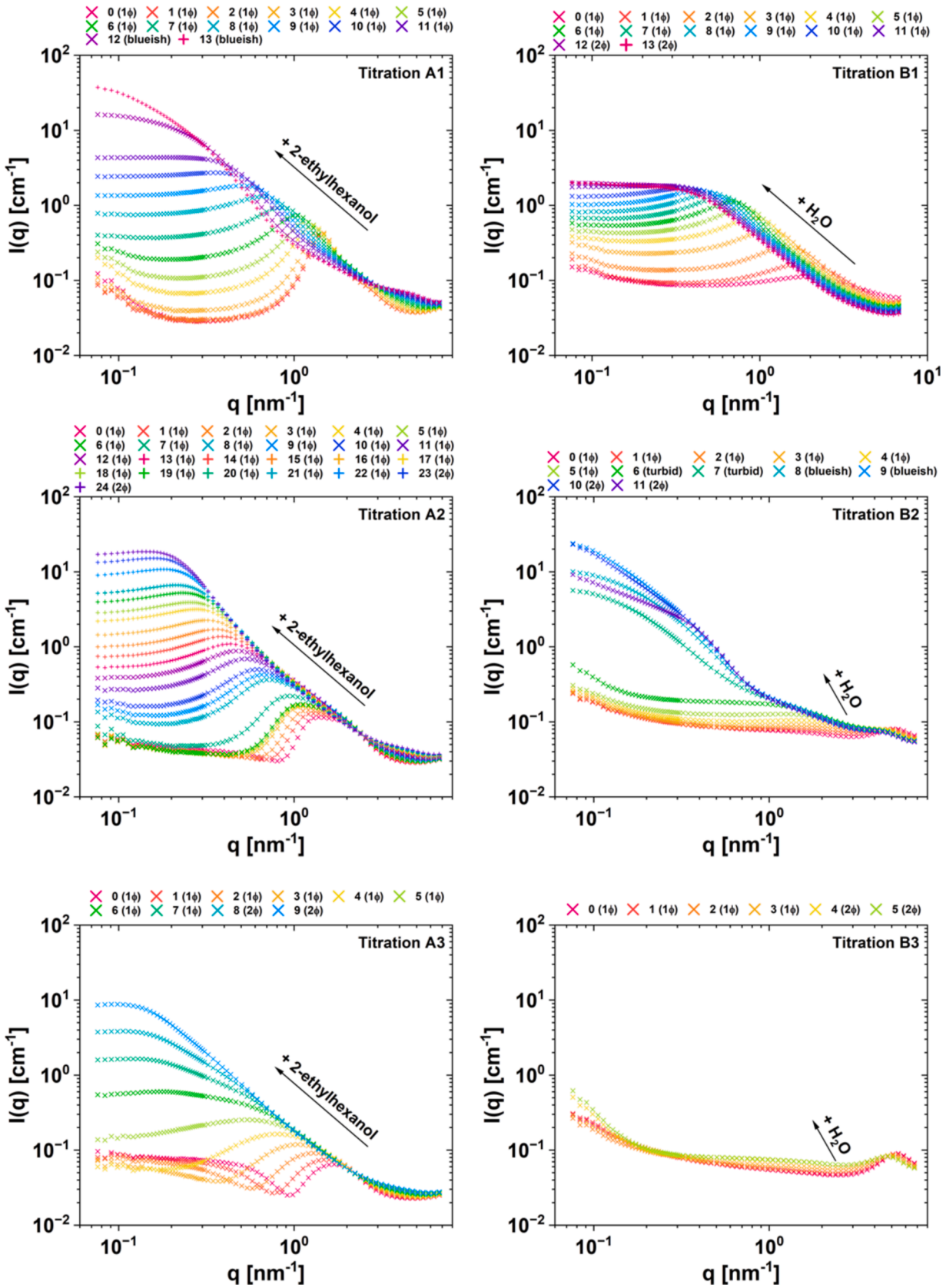

Fig. 3. SAXS spectra recorded at 25 °C along the six dilution lines indicated in the phase diagram in Fig. 2. Mainly the spectra taken in the monophasic region (1ϕ) are shown. Titration A1: Initial mixture of 63.5 wt% $C_8E_8CH_2COOH$ – 36.5 wt% H_2O titrated with 2–ethylhexanol. Titration A2: Initial mixture of 30 wt% $C_8E_8CH_2COOH$ – 70 wt% H_2O titrated with 2-ethylhexanol. Titration A3: Initial mixture of 15 wt% $C_8E_8CH_2COOH$ – 85 wt% H_2O titrated with 2-ethylhexanol. Titration B1: Initial mixture of 63.5 wt% $C_8E_8CH_2COOH$ – 36.5 wt% 2-ethylhexanol titrated with H_2O. Titration B2: Initial mixture of 30 wt% $C_8E_8CH_2COOH$ – 70 wt% 2–ethylhexanol titrated with H_2O. Titration B3: Initial mixture of 15 wt% $C_8E_8CH_2COOH$ – 85 wt% 2–ethylhexanol titrated with H_2O.

in shape to those observed in the Onuki region during titration B2 (samples B2-8 and B2-9), showing that samples A1-12 and A1-13, exhibiting only a slightly blueish appearance, are within the Onuki region (as indicated in Fig. 2).

The dilutions of the oil-rich samples reveal a very different behavior. Instead of a bump expected for surfactant aggregates, there is hardly any scattering in titration B3. The solution is close to a regular solution, i.e., water is soluble in concentrated solutions of the surfactant in the oil. Instead of the classical inversion of O/W to W/O when moving from the left side to the right side of the triangle, we detect molecular weakly structured solutions that can be characterized more quantitatively using the scattering invariant (see below).

The first five points of titration B2 and titration B3 show a broad peak in the high-q range, around $q \approx 5$ nm^{-1}, reflecting the (polydisperse) weak W/O aggregation of 2-ethylhexanol –OH groups and surfactant headgroups. As seen in **Fig. S2**, where the scattering of 2-ethylhexanol saturated with water is compared to the spectra of titration B3, this broad peak is close to what is observed in absence of any surfactant. The peak shifts to lower q as water is added to hydrate the headgroups: The mesh size that characterizes this network increases with the number of water molecules [23]. At the same time, there is no distinct peak in the mid-q range, showing that the mixture of 2-ethylhexanol and surfactant is a molecular solution with only weak aggregation and no micelle formation. In titration B1, the broad peak is shifted to lower q, with a maximum around $q = 2$ nm^{-1}, as the mixture contains more surfactant than 2-ethylhexanol.

The initial mixtures were also measured as individual samples, i.e., independently of the auto-dilution setup. In the auto-dilution setup, minute amounts of either water or 2-ethylhexanol can leak from the tube containing the titrant. Only subtle differences between the first measurement of a titration, taken prior to any addition of titrant, and the independently measured initial mixture are detected. This is exemplary shown in **Fig. S3** for titrations A2 (**Fig. S3A**) and B2 (**Fig. S3B**). Even traces of the respective titrant led to an intensity increase in the low-q range, suggesting attraction between aggregates. This is especially seen when adding water to the binary mixture of surfactant and 2-ethylhexanol, see **Fig. S3B**.

The experimental scattering invariants obtained for titrations A1, A2, and A3 are plotted as a function of the volume ratio *V(2-ethylhexanol)/V(tail)* in Fig. 4**A**, where *V(2-ethylhexanol)* and *V(tail)* are the volumes of 2-ethylhexanol and surfactant tails in the mixture, respectively.

In the case of titration A1, where 2-ethylhexanol is added to an initial mixture of 63.5 wt% $C_8E_8CH_2COOH$ and water, a clear change of slope in the increase of the invariant with the ratio V(2-ethylhexanol)/V(tail) is observed around *V(2-ethylhexanol)/V(tail)* = 2. Therefore, we can deduce that up to *V(2-ethylhexanol)/V(tail)* = 2, corresponding to a mole ratio $s = n(2\text{-ethylhexanol})/n(tail) = 1.9$, 2-ethylhexanol is incorporated into the micellar cores, swelling the micelles. Since 2-ethylhexanol is slightly amphiphilic, the hydroxyl group can protrude into the hydrophilic micellar shell, effectively increasing the interfacial area per surfactant molecule. At higher volume ratios, the invariant remains constant, which is a consequence of the dissolution of surfactant in a 2-ethylhexanol-rich pseudo-phase. The mole ratio $s = 1.9$ can therefore be identified as a "saturation mole ratio" of the micellar cores limited by the interfacial surfactant film. Note that a similar, but much weaker, change of slope is also seen for titration A2. A plateau, however, is not reached before macroscopic phase separation occurs.

In analogy, the experimental invariants obtained for titrations B1, B2, and B3 are given as a function of the volume ratio *V(H_2O)/V(head)* in Fig. 4**B**, where *V(H_2O)* and *V(head)* are the volumes of H_2O and surfactant headgroups in the mixture, respectively. For the titrations B1 and B2, a clear change of slope is observed around *V(H_2O)/V(head)* = 0.24, corresponding to a mole ratio of water and ethylene oxide (EO) groups of $w = n(H_2O)/n(EO) = 0.6$. From this we can deduce that up to 0.6 water molecules per ethylene oxide group, water is only hydrating the headgroups. As a consequence, the fraction of non-hydrated surfactant monomers dissolved in the oil pseudo-phase decreases. Additional water molecules are still further hydrating the EO headgroups (at least up to $w \approx 1.5$) [24–28]. Added water is continuously incorporated into the hydrophilic headgroup layer, gradually decreasing the fraction of dissolved surfactant monomers. The value $w = 0.6$ is the threshold, below which the solubility of surfactant monomers in the oil phase strongly increases. As already seen in the SAXS data in Fig. 3, all surfactant is dissolved in the oil throughout the monophasic domain of titration B3. The same is true for titration B2 until the Onuki region is approached.

We attempt to fit the spectra with a Teubner-Strey three-parameter expression, as shown for titration A1 in Fig. 5. The Teubner-Strey model fits for the other titrations are given in **Figs. S4** (titration A2), **S5** (titration A3), **S6** (titration B1), **S7** (titration B2), and **S8** (titration B3). The corresponding model parameters are given in Tables **S7A, S7B** (titration A1), **S8A**, **S8B** (titration A2), **S9A**, **S9B** (titration A3), **S10A**, **S10B** (titration B1), **S11A**, **S11B** (titration B2), **S12A**, and **S12B** (titration B3). As already mentioned in section 2.5.2.2., the internal structuring and contrast of the surfactant film cannot be neglected. It produces a slope of q^{-2} in the mid-q range, which is not described by the Teubner-Strey model. Inherent to the Teubner-Strey model is the

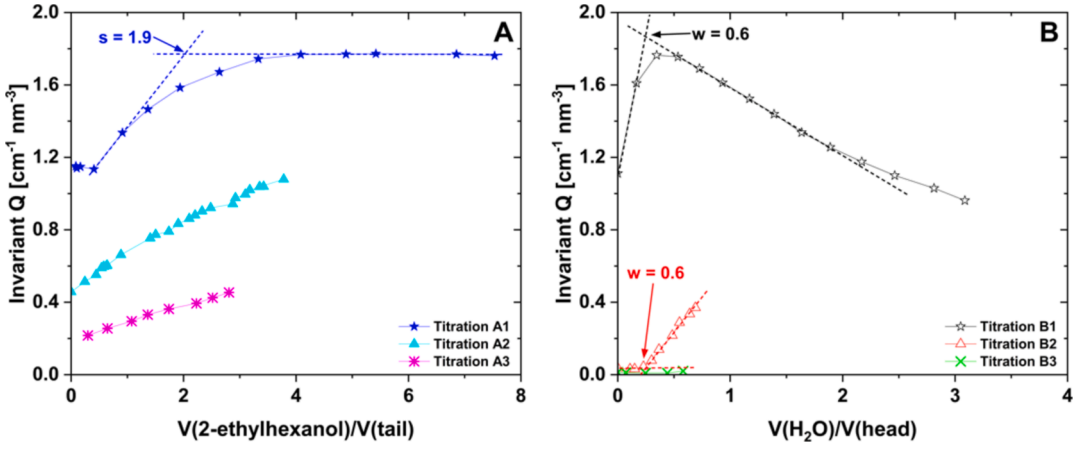

Fig. 4. Experimental scattering invariants Q obtained from the SAXS data of the monophasic samples of the six titrations indicated in the phase diagram, see Fig. 2. (A) Experimental invariants of titrations A1, A2, and A3 as a function of the volume ratio *V(2–ethylhexanol)/V(tail)*. The respective mole ratio is $s = n(2\text{-ethylhexanol})/n(tail)$. (B) Experimental invariants of titrations B1, B2, and B3 as a function of the volume ratio V(H_2O)/V(head). The mole ratio of water and ethylene oxide (EO) groups is given as $w = n(H_2O)/n(EO)$.

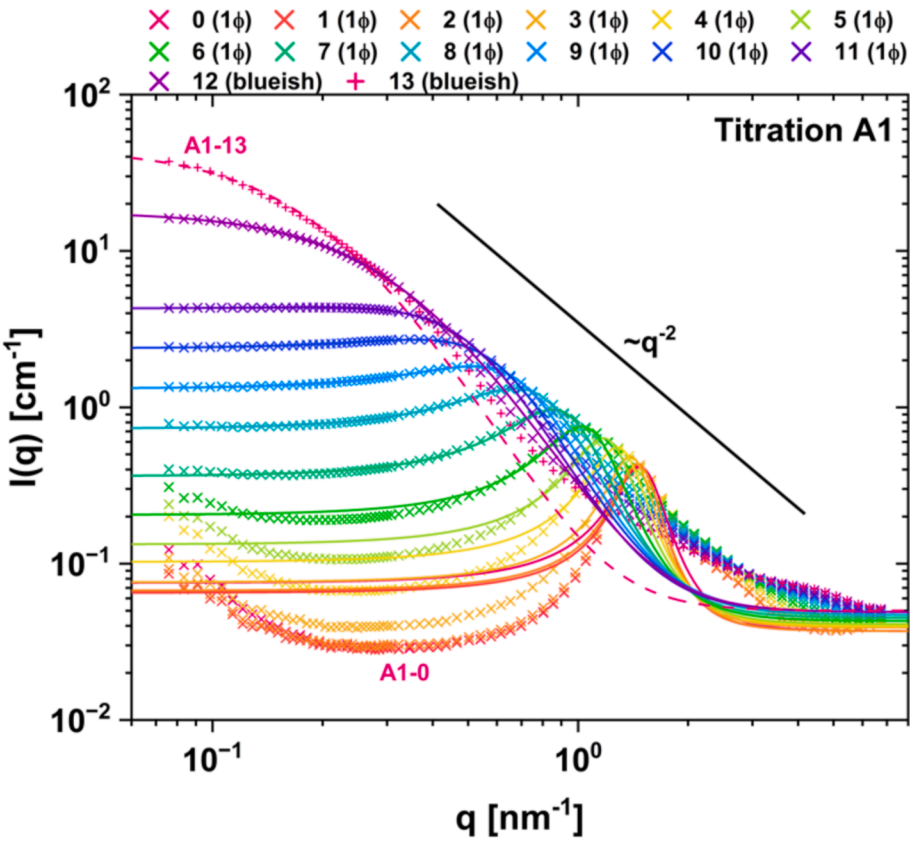

Fig. 5. Teubner-Strey model fits to the SAXS data obtained in the monophasic region along dilution line A1. Solid lines: Fitted curves. Symbols: SAXS data. The model parameters are given in **Tables S7A and S7B**. The model works well for the low-q range and the peak onset of microemulsion samples. The decline after the peak is not described by the model, as the model produces a q^{-4} decay and the scattering data typically exhibit a q^{-2} decay. A low-q upturn is found for the first few samples. The first few samples, comprising swollen "flocculated" micelles in water, are not described well by the model. Also, in the region around 2–3 nm^{-1}, failure of the Teubner-Strey model at least by a factor of 2 is evident, even when plotted in logarithmic scale.

classical q^{-4} decay found in mixtures with sharp interfaces. Here, the interface thickness is around 2 nm with a typical domain size of 3 nm, in which case neglecting the film thickness is inconsistent [29]. Consequently, the mid-q range following the peak-onset of the presented data is impossible to fit to the Teubner-Strey model, even if the low-q range and the peak onset are reproduced excellently, see Figs. 5, S4, and S6. As the same contrast dominates the whole scattering curve in the case of (swollen) core–shell micelles, whether they are flocculated (L_1/L_1' phase) or not (L_1 phase), the Teubner-Strey model is not suited to describe the scattering in such cases, see samples A1-0 to A1-4 in Fig. 5, samples A2-0 to A2-10 in **Fig. S4**, and all samples in **Fig. S5** (titration A3).

The model cannot account for the observed low-q upturn due to inter-micellar attraction, i.e., micellar flocculation, as observed in Figs. 5 **and S4**, or the "flocculation" of any other aggregates, as seen in **Figs. S6** (titration B1), **S7** (titration B2), and **S8** (titration B3). Due to the mesoscale of the pseudo-phases in the Onuki region, the Teubner-Strey model is not suited to describe the scattering produced by the two different contributions in this region, see samples B2-6 to B2-9 in **Fig. S7** and samples A1-12 and A1-13 in Fig. 5.

An important (approximate) result obtained from the Teubner-Strey model fits is the fraction of surfactant dissolved in the hydrophobic pseudo-phase B, which otherwise consists of surfactant tails and 2-ethylhexanol. The fraction of surfactant dissolved in B, $x_{surfactant,B} = \phi_{surfactant,B}/\phi(C_8E_8CH_2COOH)$, where $\phi_{surfactant,B}$ is the volume fraction of surfactant dissolved in B and $\phi(C_8E_8CH_2COOH)$ is the total volume fraction of surfactant in the sample, obtained for the fitted samples is graphically presented in **Fig. S9**. The qualitative trends are in agreement with expectation.

Since the Teubner-Strey model cannot describe well most of the obtained SAXS data, we now turn to a more refined model. Any scattering pattern is decomposed into an Ornstein-Zernike contribution and a Lorentzian Broad Peak contribution, with the possibility of a low-q divergence near the phase boundary [30].

As shown by Prévost *et al.* [11–13], this Ornstein-Zernike + Broad Peak decomposition allows good numerical fits in most situations of weak aggregation observed in ultra-flexible microemulsions (alias surfactant-free microemulsions or pre-ouzo aggregates). Ornstein-Zernike + Broad Peak model fits to the SAXS data are shown for titration A1 in Fig. 6. The respective fits to the data of the other titrations are shown in **Figs. S10** (titration A2), **S11** (titration A3), **S12** (titration B1), **S13** (titration B2), and **S14** (titration B3). The obtained model parameters are given in Tables S13 (titration A1), **S14** (titration A2), **S15** (titration A3), **S16** (titration B1), **S17** (titration B2), and **S18** (titration B3).

Generally, the Ornstein-Zernike + Broad Peak model catches most of the features of the scattering curves of microemulsion samples, e.g., samples A1-6 to A1-11 in Fig. 6. The Ornstein-Zernike + Broad Peak model captures the whole peak, not just the onset, and the decline after the peak is fitted much better than with the Teubner-Strey model. This is not a surprise, since there is one parameter more. Nevertheless, the decline in the scattering data can deviate slightly from the scattering curve described by the model due to the in-plane scattering of the surfactant film. This can be seen well in titration A2, see **Fig. S10**, where the decline is reproduced rather well for the microemulsion samples closer to the biphasic domain (A2-17 to A2-22), but rather poorly closer to the swollen micellar region (A2-11 to A2-16) since the contribution of the surfactant film to the scattering is more significant in this region.

If the scattering of a microemulsion additionally exhibits a weak

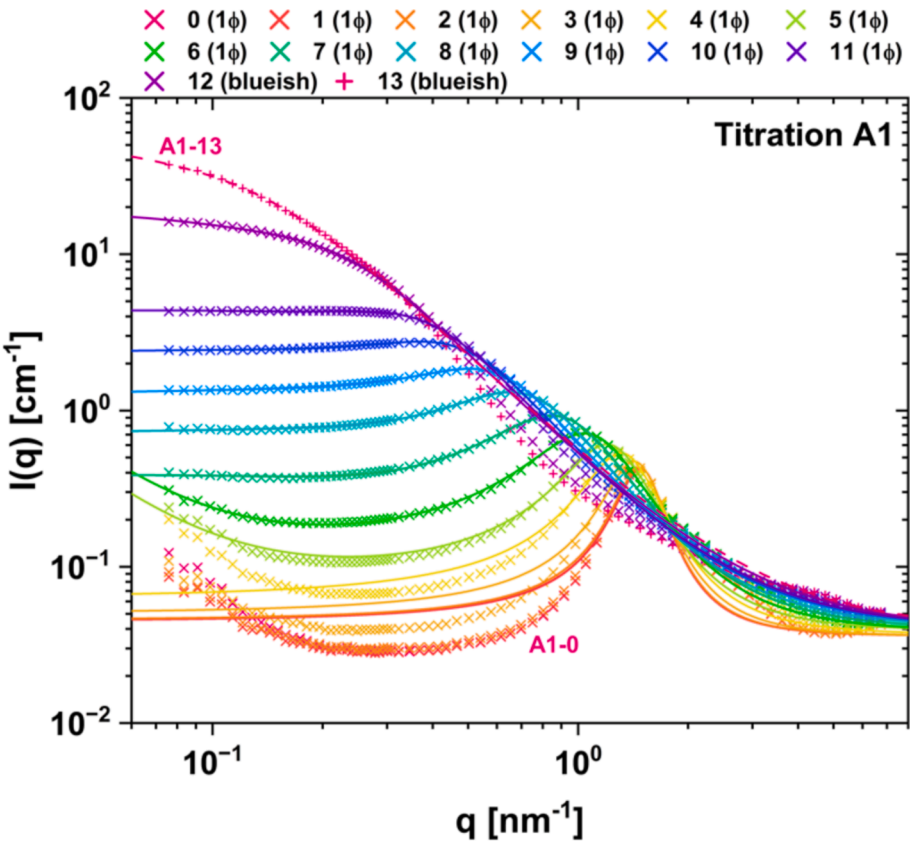

Fig. 6. Ornstein-Zernike + Broad Peak model fits to the SAXS data obtained in the monophasic region along dilution line A1. Solid lines: Fitted curves. Symbols: SAXS data. The model parameters are given in **Table S13**. The model works well for the microemulsion samples. Though the model works better for the decline after the peak than the Teubner-Strey model, the decline is not fully captured by the model. The first few samples, comprising swollen "flocculated" micelles in water, are not described well by the model.

peak at high-q due to the weak aggregation of the hydroxyl groups of a 2-ethylhexanol-rich pseudo-phase, e.g., samples A1-10 and A1-11 in Fig. 6, the model cannot reproduce this peak. An additional Broad Peak contribution would be required. The Ornstein-Zernike + Broad Peak model cannot describe the scattering produced by ("flocculated") core–shell micelles due to the contribution of the core–shell form factor, as seen for the first few samples of titrations A1 (Fig. 6) and A2 (**Fig. S10**), and especially for titration A3 (**Fig. S11**), where the form factor dominates the scattering.

On the contrary, all scattering curves of titration B1, where the initial binary mixture of 63.5 wt% $C_8E_8CH_2COOH$ and 36.5 wt% 2-ethylhexanol comprises relatively similar polar and apolar volume fractions, can be described excellently with this model, see **Fig. S12**. In titration B2, where the initial binary mixture of 30 wt% $C_8E_8CH_2COOH$ and 70 wt% 2-ethylhexanol is dominated by the oil, more than half of the surfactant is dissolved in the oil. The non-dissolved surfactant either participates in the weak aggregation of the alcohol or forms other weak surfactant-rich aggregates. The weak aggregation of the alcohol, i.e., the hydrogen-bonded –OH network, including the participating surfactant headgroups produces a broad peak at high-q. The small fraction of surfactant forming other weak surfactant-rich aggregates on the other hand contributes to the scattering in the mid-q range. A low-q upturn due to random clustering is also observed as soon as water is added to the system. As shown in **Fig. S13**, the four-parameter model cannot describe the entire scattering curve simultaneously. One can either model the low-q upturn and the mid-q range, but not at all the high-q broad peak (samples B2-3 to B2-5), or one can model the high–q broad peak and the mid-q range, but not at all the low-q upturn (samples B2-0 to B2-2). The same is true for titration B3, where initially (almost) all surfactant is dissolved in the oil. In the case of titration B3, the latter approach is shown, see **Fig. S14**.

Of course, the Ornstein-Zernike + Broad Peak model is not suited either to describe the scattering curves produced inside the Onuki region (samples A1-12 and A1-13 in Fig. 6 and samples B2-6 to B2-9 in **Fig. S13**), as the two mesoscale pseudo-phases in equilibrium are themselves structured solutions, and one is not able to account for all the contributions with this model.

The peak positions are linked to the average repeat distance $D^* = 2\pi/q_{peak}$ of the structures producing the peak. In Fig. 7**A, D*** is given for all titrations as a function of the nonpolar volume fraction $\phi(nonpolar)$, which is not simply the combined volume fraction of the surfactant tails and 2-ethylhexanol, but includes any species that is dissolved in the nonpolar pseudo-phase. $\phi(nonpolar)$ is equivalent to the volume fraction of pseudo-phase B, $\phi_B = 1\text{-}\phi_A$, as calculated according to eqs. S2.7 or S2.11 (see **Note S2**) when applying the Teubner-Strey model. The only unknown parameter significantly influencing $\phi(nonpolar)$ is the fraction of the surfactant volume dissolved in the nonpolar pseudo-phase B, $x_{surfactant,B}$, which was approximately inferred from the Teubner-Strey model fits, as described earlier in this section. The peak positions given for titration B3 and the first three samples of titration B2 reflect the position of the broad peak produced by the hydrogen-bonded –OH network of mainly the alcohol and cannot be directly compared to the other peak positions due to their different origin.

From the changes of the typical size D^* as a function of $\phi(nonpolar)$ alone, one cannot learn much about the system, except that there is no sign of a sudden phase inversion. To learn more, a swelling plot of the reduced peak position ΣD^* versus $\phi(nonpolar)$, as shown in Fig. 7**B**, must be determined. ΣD^* is unitless, as the peak position D^* is multiplied with the specific surface area, i.e., the interfacial area per unit volume, Σ. In the case of two domains with sharp interfaces, Σ could be determined

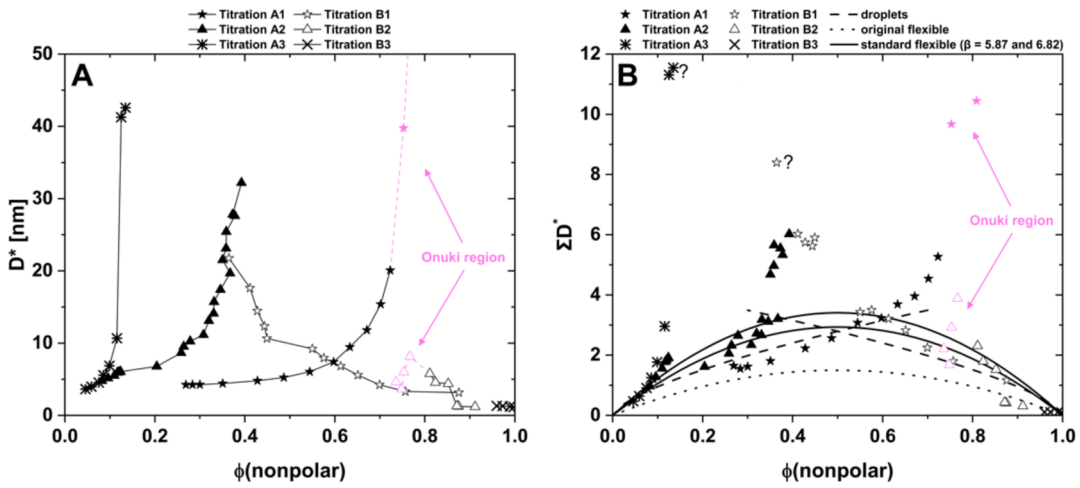

Fig. 7. (A) Repeat distance $D^* = 2\pi/q_{peak}$ of all monophasic samples as a function of the nonpolar volume fraction. The peak position is inferred from the Ornstein-Zernike + Broad Peak model fits (Fig. 6 and S10 to S14 and **Tables S13 to S18**). The nonpolar volume fraction includes surfactant dissolved in the oil pseudo-phase and equals the volume fraction of pseudo-phase B in the Teubner-Strey model (Fig. 5 and S4 to S8 and **Tables S7A to S12A**), where $\phi_B = 1\text{-}\phi_A$. (B) Swelling plot of the reduced peak position ΣD^* as a function of the nonpolar volume fraction. D^* and *ϕ(nonpolar)* are the same as in (A). Σ [nm^2/nm^3] is the surface area of the interface per unit volume, obtained using eq. (20). For reference, theoretical curves of repulsive droplets, the original flexible model, and the standard flexible model (with β = 5.87 and β = 6.82) are shown. Points measured inside the Onuki region are also highlighted in magenta. The Onuki effect produces fewer but much larger aggregates due to solubilization of quasi-critical fluids at mesoscale by the surface-active component(s). The points indicated by a question mark show extraordinarily high values of ΣD^*, which is most likely a result of critical fluctuations close to the phase boundary. The swelling plot in reduced units reveals all samples that show a biliquid foam structure ($4 < \Sigma D^* < 6$). (For interpretation of the references to colour in this figure legend, the reader is referred to the web version of this article.)

using the Porod limit of the scattering [31]

$$I(q) = \frac{P}{q^4} + background, \tag{15}$$

where the Porod constant P is given by

$$P = \frac{\Sigma}{2\pi\Delta SLD_{1|2}{}^2} + background, \tag{16}$$

and the scattering invariant

$$Q_{th} = 2\pi^2\phi_1(1-\phi_1)\Delta SLD_{1|2}{}^2, \tag{17}$$

so that

$$\Sigma = \frac{P}{Q_{th}}\pi\phi_1(1-\phi_1). \tag{18}$$

If the Porod limit of the data can be fitted to eq. (15) to obtain P, and the volume fractions are known, the specific surface Σ can be calculated after determining the scattering invariant. If the system contains a surfactant, the interface has a certain thickness, and the observed slope can be smaller than q^{-4}. This can be accounted for, using the Kirste-Porod correction, as done for example by Schmidt et al. [32] (shown in their Supplementary Information).

$$I(q) = \frac{P}{q^4}\left(1 + \frac{C}{q^2}\right) + background, \tag{19}$$

where C depends on the local principal curvatures of the surface. To then use eq. (18), the contrasts also must be suitable for a two-component approximation, i.e., the internal contrast of the surfactant film must be negligible compared to the contrast of the two phases separated by the surfactant film. In the present system, however, this approach cannot be used because the surfactant film is not homogeneous and, as discussed in section 2.5.2.2., the internal contrast of the surfactant film is too large. The observed slope is around q^{-2} and a fit to eq. (19) would yield unphysical results, as the intrinsic scattering of the surfactant film contributes to the scattering in the same q-range, but is not accounted for in the model. Further, the intrinsic contrast of the surfactant film is not accounted for in the two-component approximation, making eq. (17) also erroneous. Obtained values of Σ would therefore be wrong.

In the simplest case, where the interfacial film is solely made of all available surfactant molecules in the system, $\Sigma = N_s \cdot a_s$, where N_s is the number density of surfactant and a_s is the area per surfactant molecule. Since 2-ethylhexanol can act as a co-surfactant and be incorporated into the surfactant film and the surfactant can dissolve in 2-ethylhexanol, the best experimental estimation of the total W/O contact area per unit volume Σ is

$$\Sigma = \frac{\phi_{surfactant} \cdot \left(1 - x_{surfactant,B}\right) \cdot \rho_{surfactant} \cdot N_A}{M_{surfactant}} \cdot a_{s,eff}, \tag{20}$$

where N_A is the Avogadro constant and $a_{s,eff}$ is the effective area per surfactant molecule accounting for the additional area provided by the 2-ethylhexanol molecules in the surfactant film. Since $x_{surfactant,B}$ is known approximately from the Teubner-Strey fits (Tables S7A to S12A) and all other parameters are known (Tables 1 to 6 and **Note S1**), the only missing parameter is $a_{s,eff}$. In this work, we estimate that $a_{s,eff} = 1.80$ nm^2 (see discussion in **Note S3**).

The obtained values for ΣD^*, shown as a function of *ϕ(nonpolar)* in Fig. 7**B**, can be compared to several predictive theoretical models for the structure of microemulsions, the predicted lines of which are also shown in Fig. 7**B**. For the case of non-coalescing W/O or O/W droplets, the expected average repeat distance can be calculated in a good approximation according to [33]

$$D^* = \frac{\sqrt{2}}{1.225 \cdot \sqrt[3]{N}}, \tag{21}$$

where the number density of droplets N is given by $\phi = N \cdot 4\pi R^3/3$, R being the droplet radius. The specific surface area is in this case given by $\Sigma = N \cdot 4\pi R^2$. The reduced peak position ΣD^* is then given by

$$\Sigma D^* = 4.431 \cdot \phi^{\frac{2}{3}}. \tag{22}$$

According to the original flexible model [34,35], the product ΣD^* in the case of a random dispersion of flexible interfaces without any local curvature constraint is given as

$$\Sigma D^{*} = 6 \cdot \phi \cdot (1 - \phi). \quad (23)$$

Note that the model was proposed by Jouffroy, Levinson, and de Gennes [35] using a tessellation of cubic random cells, inspired by the Voronoi tessellation used by Talmon and Prager [36] to describe the structure of microemulsions. In the original flexible model, the effective repulsion between local domains of either pseudo-phase is not taken into account. If the alternation of water and oil domains is considered, a factor of 2 is introduced in eq. (23). Additionally, the factor of 6 is replaced by a numerical factor β, where $5.87 \leq \beta \leq 6.82$, to give the standard flexible model

$$\Sigma D^{*} = 2 \cdot \beta \cdot \phi \cdot (1 - \phi). \quad (24)$$

A further refinement of those models was introduced by Zemb *et al.* [37] in the form of the DOC (Disordered Open and Connected) model, where all possible microstructures can be generated based on the Voronoi tessellation. Each Voronoi cell is filled by a direct or a reverse micelle (DOC sphere model), by part of a giant cylindrical micelle (DOC cylinder model), or by a swollen bilayer (DOC lamellar model). In terms of the reduced peak position ΣD^{*}, the predictions of the DOC sphere and cylinder models are within the region covered by the standard flexible model, and the DOC lamellar model predicts values of ΣD^{*} between around 3 and 4, as shown for example in ref. [15]. The DOC lamellar model also describes sponge phases.

When comparing the data to the theoretical models in Fig. 7**B**, it must be noted that for titration B3 and the first three points of titration B2, D^{*} was taken from the high-q broad peak originating from the hydrogen-bonded –OH network of the alcohol (plus surfactant). As this peak is not directly linked to the specific surface area of a surfactant film, the values of ΣD^{*} in these cases should not be interpreted. Further points that should not be interpreted within the framework of the swelling plot, shown in Fig. 7**B**, are those shown in magenta, which represent data measured in the Onuki region, as the scattering in these cases is similar to that of a biphasic sample.

Since the peak seen in the scattering of the first five samples of titration A3 is mainly a form factor, the extracted value of D^{*} is not the actual repeat distance (to be extracted from the structure factor). The actual value of D^{*} should be slightly higher, which would also increase the product ΣD^{*}. For A3-0, the real D^{*} is expected to be around 6.4 nm [38], which is by a factor of around 1.75 larger than the (wrong) D^{*} given here. As a consequence, ΣD^{*} is in reality also by a factor of 1.75 larger than shown. This would produce values of ΣD^{*} slightly larger than those predicted by the different models. It is known that initially spherical core–shell micelles are dispersed in water [2], and the seemingly larger reduced peak position compared to the repulsive droplets model could originate from a rather attractive nature of the intermicellar interactions. The reason for the continuous increase of ΣD^{*} in titration A3 is most likely an underestimation of the fraction of surfactant dissolved in the oil, which is taken to be $x_{surfactant,B} = 0$ from the Teubner-Strey model fits. Since the model is not adequate to describe the scattering of oil-swollen core–shell micelles, this is probably not true, and $x_{surfactant,B}$ is expected to slightly increase, which would in turn slightly decrease Σ. The same is true for the increase observed for the first few points of titration A2, samples A2-0 to A2-6, which in this case is clearly indicated by the apparent "sudden" increase of $x_{surfactant,B}$ from 0 to 0.3325 according to the Teubner-Strey fits from sample A2-6 to A2-7, see **Table S8A**. Thus, the observed increase of ΣD^{*}, not conforming to any model prediction, is an "artifact" due to a lack of good approximations of $x_{surfactant,B}$ in these cases. The points indicated by a question mark have a very large value of ΣD^{*}, much larger than any model would predict, which is most likely a consequence of critical fluctuations close to the phase boundary.

If $x_{surfactant,B}$ would be extrapolated between $x_{surfactant,B} = 0$ for sample A2-0 and $x_{surfactant,B} = 0.3325$ for sample A2-7, the first eight points of titration A2 in Fig. 7**B** would more or less follow the line predicted by the repulsive droplets model, as expected for swollen core–shell micelles. The following points of titration A2 are located within the region predicted by the standard flexible model until a further increase of ΣD^{*} up to around $\Sigma D^{*} = 6$ is observed. If adequate approximations of $x_{surfactant,B}$ were available for titration A3, the points would be expected to more or less follow the line predicted by the repulsive droplets as well, until critical fluctuations apparently increase ΣD^{*}. The points obtained for titration A1 initially also follow the line predicted by the repulsive droplets model, as expected for the slightly interdigitated core–shell micelles in the L_1/L_1' phase. Above sample A1-7, a continuous increase of ΣD^{*} up to around 5.3 is observed. The points of titration B1 initially also seem to follow the theoretical line of repulsive droplets, suggesting that the surfactant dominated surfactant – 2-ethylhexanol mixture may be described as polar droplets in the apolar phase. Since more than half of the surfactant is not participating in aggregation ($x_{surfactant,B} > 0.5$) and the dehydrated surfactant is miscible with 2-ethylhexanol, the aggregation is expected to be weak, somewhat similar to the hydrogen bonded networks formed by alcohols [13]. As more water is added, ΣD^{*} increases into the range of the standard flexible model as the initially (statistically) separated "droplets" start to connect to more and more form some sort of "network", i.e., hydrophilic channels. While these structures are in principle reverse (W/O), these structures are only weakly aggregated and not stable reverse micelles. Beyond sample B1-6, ΣD^{*} sharply increases to 5.6–6.0.

There clearly is a region between $4.7 \leq \Sigma D^{*} \leq 6.0$ in the swelling plot shown in Fig. 7**B**, where all points measured in a specific region in the middle of the phase diagram extending towards the water-rich corner are located. These values of ΣD^{*} are up to twice as large as expected for sponge phases (usually $\Sigma D^{*} \approx 3$), meaning there must be up to double the interfacial area per unit volume.

4. Discussion

The phase diagram of the ternary system 2-ethylhexanol – $C_8E_8CH_2COOH$ – H_2O, shown in Fig. 2, is a borderline case between ultra-flexible microemulsion systems and flexible microemulsion systems. This can be expected for the $C_8E_8CH_2COOH$ surfactant, which itself may be viewed as a borderline case between a surfactant and a hydrotrope. It does not exhibit a triphasic domain or any liquid crystalline phases typical of a classical flexible microemulsion system, but in contrast to ultra-flexible microemulsion systems there is clear structuring with a surfactant film and not just weak pre-clusters as observed for ultra-flexible microemulsions, often also called surfactant-free microemulsions if the amphiphilic compound is a hydrotrope [15,39,40]. The identification of the microstructures was possible through analysis of SAXS data along six dilution lines in the phase diagram. The scattering invariant, model fits, and the construction of a swelling plot of the reduced peak position as a function of the nonpolar volume fraction are used. As shown in section 3, the Teubner-Strey model fits cannot reproduce the mid-q ranges of the scattering curves due to intrinsic scattering contrast of the surfactant film. However, they allow us to derive an approximate value for the fraction of surfactant dissolved in the oil pseudo-phase, a quantity that is otherwise unknown and cannot be measured even by local characterization such as NMR relaxation or spin-echo. Ornstein-Zernike + Broad Peak model fits work better than the Teubner-Strey fits, but also deviate in the region of the Porod limit due to the complex surfactant film contrast.

Apart from the biphasic domain and the large isotropic monophasic domain, there is only one small region near the critical point that appears milky or blueish in the "middle" of a single-phase region, not only adjacent to phase separation or the critical point. A small portion of this Onuki region, furthest from the critical point towards the binary mixture of surfactant and 2-ethylhexanol, appears as a turbid mixture. As more water is added, the turbidity vanishes and only a blueish appearance due to the Tyndall effect remains, indicating that the droplet size decreases. Despite the presence of droplets large enough to cause a turbid

appearance, this region is not thermodynamically biphasic, but a single thermodynamically stable phase. The Onuki region is a thermodynamically stable dispersion of one pseudo-phase in another, where both pseudo-phase domains are of mesoscale size, i.e., up to several hundreds of nanometers in size. Since the domains are mesoscaled and the mixture is thermodynamically stable, it may be referred to as "mesoscale solubilization". A. Onuki initially explained this phenomenon in the case of water – oil mixtures including antagonistic salts, where one ion is hydrophilic and the counterion is hydrophobic [19,20]. In this case, the antagonistic salt reduces the interfacial tension due to the formation of electric double layers around water – oil interfaces, because one ion prefers to be solvated in water and one ion is dissolved in the oil. Since charge neutrality must be preserved in the bulk, the two ion species remain in relatively close proximity to each other around the interface. Near solvent criticality this effect makes the interfacial tension theoretically negative, which results in an increase of the interfacial area and to microphase separation, i.e., a thermodynamically stable mesoscale phase separation. Often, interfaces are formed also within the dispersed pseudo-phase, i.e., one droplet may contain multiple interfaces [20,41]. Macroscopic phase separation is not possible, as the charge neutrality must be preserved. Okamoto and Onuki [21] later also explained this effect in the case of a ternary nonionic system of oil – water – alcohol, where the role of the antagonistic salt is taken by the amphiphilic nature of the alcohol. In the present system, the nonionic surfactant $C_8E_8CH_2COOH$ has a hydrophobic C_8 chain covalently bound to the hydrophilic headgroup, therefore having a tendency to go to the 2-ethylhexanol-water interface. 2–ethylhexanol can dissolve the surfactant in its dehydrated state. As water is added, the hydrated headgroups are no longer soluble and microphase separation is energetically favored to create 2-ethylhexanol-water interfaces.

The dilution line of titration A1 starts in the L_1/L_1' phase, known from previous work [1,2], formed by the binary mixture of 63.5 wt% surfactant and 36.5 wt% water and extends towards the 2-ethylhexanol-rich corner. It crosses the blueish part of the Onuki region and enters the biphasic domain at the critical point. The first few samples A1-0 to A1-4 can be clearly identified as a (swollen) L_1/L_1' phase, i.e., (swollen) densely packed micelles with partial headgroup interdigitation, just by comparing the scattering curves in Fig. 3. The following scattering curves indicate a continuous transition to another microemulsion structure, which is, as will be shown in the following, the biliquid O/W nanofoam phase. Inside the Onuki region (samples A1-12 and A1-13), two different contributions to the scattering can be identified. In the q range up to $q \approx 1\ nm^{-1}$, the scattering of the pseudo-phase dispersed as droplets is dominant, while at higher q the scattering of the pseudo-phase in which the droplets are dispersed dominates. Fits of the lower q part to the Ornstein-Zernike + Broad Peak model, suggest correlation lengths between around 8 nm and 16 nm. Since the scattering is not fully describable with this model, these values should only be taken as a

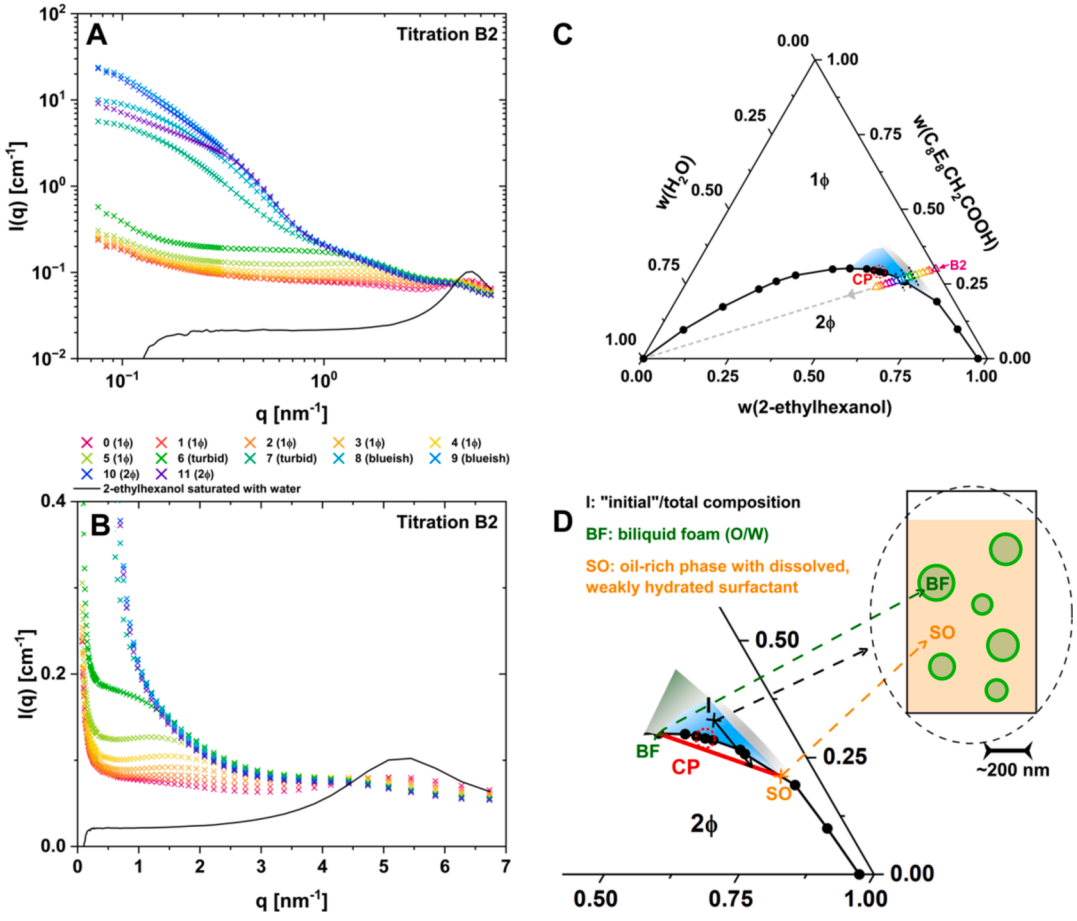

Fig. 8. (A) SAXS data recorded during titration B2 in log–log scale. (B) The same data presented in lin-lin scale, cutting off the higher intensities at low-q. The solid black line represents data of 2-ethylhexanol saturated with water. (C) The points measured during titration B2 are shown in the phase diagram of the ternary system 2-ethylhexanol – $C_8E_8CH_2COOH$ – H_2O at 25 °C. The part of the Onuki region with a turbid appearance is shown in grey, while the part with a slightly blueish appearance is shown in blue. (D) The principal method of estimating the "microphase separated" pseudo-phase compositions and volume fractions in the phase diagram, see text. A schematic drawing of the biliquid nanofoam ("BF") dispersed in the 2-ethylhexanol-rich phase containing dissolved, weakly hydrated surfactant (surfactant in oil – "SO") inside the Onuki region is also shown. (For interpretation of the references to colour in this figure legend, the reader is referred to the web version of this article.)

rough estimate of the order of magnitude of the droplet size. The two different contributions are best seen in titration B2, crossing both the turbid and the blueish parts of the Onuki region coming from the binary mixture of 30 wt% surfactant and 70 wt% 2-ethylhexanol adding water. The recorded scattering of the first turbid sample B2-6 shows mainly a contribution of the continuous pseudo-phase, but also a Porod asymptotic behavior of the contribution of the dispersed pseudo-phase at low-q, see Fig. 8**A and 8B**. The dilution line B2 is also shown in the phase diagram in Fig. 8**C**. This means that the droplets in this case must be larger than 100 nm. Ornstein-Zernike + Broad Peak model fits suggest micron-sized droplets. However, the error of this size approximation may be significant. As more water is added, the droplet size decreases towards sample B2-9, shifting a larger portion of the droplet pseudo-phase contribution into the measured q range. The typical droplet size in the blueish region is then much smaller than 100 nm. As seen in the scattering curve of samples B2-6 to B2-9, see Fig. 8**A and 8B**, the continuous pseudo-phase in the Onuki region that is in equilibrium with large droplets of a ternary water-rich composition exhibits a broad peak at high-q, which can be assigned to weak aggregation of the alcohol into hydrogen bonded –OH networks with some participation of surfactant headgroups and water [13]. Such a broad peak is also seen in almost pure 2-ethylhexanol saturated by water, see solid black line in Fig. 8**A and 8B**. The scattering contribution of the continuous phase closely resembles the scattering of sample B2-5, where a large fraction of the surfactant is dissolved in 2-ethylhexanol. While the oil-rich phase with dissolved surfactant is adjacent to the Onuki region on the oil-rich side, the O/W biliquid nanofoam region (see next paragraph) is adjacent to the Onuki region on the other side towards the middle of the phase triangle. Thus, we know that in the Onuki region droplets of the biliquid nanofoam ("BF") phase with sizes up to several hundreds of nanometers are dispersed in an oil-rich phase containing dissolved, weakly hydrated surfactant ("SO"), as schematically drawn in Fig. 8**D**. Inside the Onuki region, O/W interfaces are created. As described above, a fraction of the surfactant (and some 2-ethylhexanol as co-surfactant) is "consumed" to form the surfactant films. Therefore, one can estimate the compositions of the two separating pseudo-phases using the true two-phase region of the phase diagram, as also shown in Fig. 8**D**. For an "initial" total composition inside the Onuki region ("I") one can draw an arrow in the phase triangle towards the first tie-line (solid red line) connecting points located outside of the Onuki region. If only surfactant is required to form the surfactant film, the arrow would point towards the 2-ethylhexanol corner. Since in this case 2-ethylhexanol partially acts as a co-surfactant and is also "consumed" to from the interfacial films, the arrow points a bit more towards the binary 2-ethylhexanol – water line. The tie-lines yield a good estimate of the compositions of the two pseudo-phases and with the crossing point of the tie-line and the drawn arrow, once could estimate the volume fractions of the two pseudo-phases.

For titration A1, the scattering invariant, see Fig. 4**A**, yields a value for the saturation of the surfactant film with 2-ethylhexanol, $s_{sat} = n_{sat}(2\text{-}ethylhexanol)/n(tail) = 1.9$, meaning that a maximum of 1.9 2-ethylhexanol molecules per surfactant are incorporated as co-surfactant into the surfactant film. Any additional 2-ethylhexanol then must be incorporated into the micellar core. The Teubner-Strey model is found to describe well the low-q part and the peak onset only if $s > s_{sat}$, i.e., once there is an oil-rich phase swelling the micelles. In the case of titration A1 the condition $s > s_{sat}$ is fulfilled starting with sample A1-7, see Fig. 5. The same is true for the Ornstein-Zernike + Broad Peak model, see Fig. 6, though it yields better fits than the Teubner-Strey model in general.

This is also reflected in the swelling plot (ΣD^* vs. $\phi(nonpolar)$), see Fig. 7**B**., where the points start to deviate from the prediction of the repulsive sphere model around sample A1-7 ($\phi(nonpolar) \approx 0.6$). Interestingly, ΣD^* increases continuously up to $\Sigma D^* \approx 5.3$, which is significantly larger than a value of around 3.0 expected for bicontinuous, locally flat sponge phases [15]. $\Sigma D^* = 6$ is expected for an ideal biliquid nanofoam, where in the Voronoi tessellation treatment [42] all Voronoi cells are completely covered by surfactant bilayers, instead of only 50 % in the symmetric sponge phase. This means that deformed droplets are fully enclosed and separated by locally flat surfactant bilayers. Such a structure was first observed by Wolf *et al.* [43–45] on adding small amounts of oil to an oil-free sponge phase (L_3 phase), which they called "high-internal phase microemulsion" (HIPME). An explanation and confirmation of this transition was recently given by Menold *et al.* [46,47]. Such a biliquid nanofoam structure can be viewed as a "super-swollen" dispersion of micelles. In the systems of Wolf *et al.* and Menold *et al.*, the surfactant bilayers form hydrophobic films separating hydrophilic droplets, i.e., they observed a W/O biliquid nanofoam or "super-swollen reverse micellar phase" [46]. A W/O biliquid nanofoam consists of closely packed polyhedral aqueous nanodroplets (typically < 50 nm in size), i.e., biliquid foam cells, confined by surfactant films. The polar headgroups protrude into the aqueous pseudo-phase and the apolar chains of neighboring cells form hydrophobic bilayers swollen by oil. The polar pseudo-phase is therefore discontinuous, while the apolar pseudo-phase is continuous. In our system, the bilayers must be the reverse, i.e., hydrophobic nanodroplets are separated by a hydrated headgroup layer, forming an O/W biliquid nanofoam. There is no bulk water, as water is hydrating the headgroups, and there is a continuous transition from direct swollen micelles to the biliquid nanofoam on addition of oil, without any sign of a phase inversion. One can expect around three water molecules to be at least weakly bound to the headgroup per EO group. In titration A1, $w = n(H_2O)/n(EO) = 2.16$, and even if the surfactant molecules dissolved in the hydrophobic pseudo-phase (around 50 % of the surfactant) were completely dehydrated, there would only be around four water molecules per EO group. In addition, a reverse structure would be highly unexpected compared to a direct structure with the very hydrophilic $C_8E_8CH_2COOH$ surfactant.

The same observations are made for titration A2, the dilution line of which starts in the core–shell micellar L_1 phase [1,2] in the binary mixture of 30 wt% surfactant and 70 wt% H_2O and extends towards the 2–ethylhexanol corner. In contrast to titration A1, titration A2 does not cross the Onuki region. $s > s_{sat}$ is reached around sample A1-11, which again is where the model fits start to work much better, see **Figs. S4 and S10**. In this region, the points in the swelling plot (Fig. 7**B**) deviate from the theoretical line of repulsive droplets and are located inside the range predicted by the standard flexible model, which may indicate that the droplet sizes and shapes become increasingly random. Samples A2-14 to A2-16 exhibit ΣD^* values around 3, before the next point seemingly "jumps" to $\Sigma D^* \approx 4.7$. ΣD^* then increases up to around $\Sigma D^* = 6$ at samples A2-22, demonstrating that an O/W biliquid nanofoam is formed.

It should be noted that the possibility of a biliquid foam structure for microemulsions was discussed, to the best of our knowledge for the first time, 40 years ago by Chen *et al.* [48] and Evans *et al.* [49] in ternary systems of *n*-alkane – didodecyldimethylammonium bromide (DDAB) – H_2O. Chen *et al.* measured unexpected conductivity at very low water content, meaning that the minority phase is continuous, and discussed the possibility of an O/W biliquid nanofoam structure, i.e., a rhombododecahedral packing of polyhedral droplets, based on a high internal phase emulsion structure analysis by Lissant [50,51] using purely geometrical considerations. However, Chen *et al.* also stated the possibility that both pseudo-phases may be continuous, i.e., that the structure is bicontinuous. Two years later, Evans *et al.* concluded that the microemulsions are bicontinuous. It was shown later that the vast majority of stiff microemulsions, "stiff" meaning that the bending constant versus the packing parameter is larger than 10 $kJ \cdot mol^{-1}$ [29], including those examined by Chen *et al.* and Evans *et al.*, are modelled successfully with the DOC cylinder model as being close to connected cylinders with a variable connectivity Z [52]. Their observation of decreasing conductivity on addition of water to the water-poor microemulsion was also shown to be an effect with a general explanation within the framework of the DOC model, taking into account the constraint of fixed volume,

fixed area per molecule, and minimal curvature frustration [42]. Such a reduction of the conductivity is absent if tetradecane is used as a non-penetrating oil [48,49], in which case the structure consists of DOC lamellae [53], i.e., randomly folded oil-swollen bilayers, also known in the literature as asymmetric sponge phase [54]. Both DOC cylinder and DOC lamellar structures do not exhibit foam-like Plateau borders. Even in the DOC lamellar case, the scattering peak position shows that there are no closed domains of oil in a structure resembling a nanofoam. To the best of our knowledge, the structure described in this paper is the first O/W biliquid nanofoam.

The O/W biliquid nanofoam reported in this work is a micro-emulsion, and therefore an equilibrium structure. Metastable O/W biliquid foams with a similar foam-like structure but on a much larger scale (micron sized droplets) were already reported 25 years ago by Sonneville-Aubrun et al. [55], who obtained these "high internal phase emulsions (HIPEs)" by centrifugation of emulsions. In contrast to the thermodynamically stable O/W biliquid nanofoam reported here, the HIPEs are, as already stated by the authors, metastable emulsions.

Along the dilution line of titration A3, starting in the core–shell micellar L_1 phase [1,2] in the binary mixture of 15 wt% surfactant and 85 wt% H_2O and extending towards the 2–ethylhexanol corner. In this case, $s > s_{sat}$ is reached at sample A3-5, where at least the Ornstein-Zernike + Broad Peak model starts to give a relatively good fit to the data, see **Fig. S11**. In this case, no transition to a biliquid nanofoam can be confirmed.

The dilution line of titration B1 starts at the binary mixture of 63.5 wt % surfactant and 36.5 wt% 2–ethylhexanol and extends towards the water corner of the phase diagram. Along this dilution line, s is only slightly larger than s_{sat} and both models work quite well, see **Figs. S6 and S12**. As can be inferred from **Table S10A, a** significant fraction of the dehydrated surfactant is dissolved in the nonpolar pseudo-phase, which is a hint that the aggregation is weak. The initial microstructure may be described as weak aggregation of surfactant headgroups and alcohol –OH groups, possibly similar to the hydrogen-bonded networks formed by alcohols [13]. Initially, these fluctuations or weak aggregates seem to follow the theoretical line of the repulsive droplets model (Fig. 7**B**), suggesting that the statistically distributed weak aggregates could be described as droplets. As more water is added, the points increasingly deviate from this predicted line and are located in the range predicted by the standard flexible model, as would be expected if the extent of weak aggregation increases and leads to the formation of a network-like structure of hydrophilic "channels". The experimental scattering invariants of both titrations B1 and B2, see Fig. 4**B**, show a clear change of slope around $w_{sat} = 0.6$, which is interpreted as the maximum hydration, i.e., the maximum number of water molecules per EO group, above which the surfactant's solubility in 2-ethylhexanol decreases drastically. Samples B1-5 and B1-6 exhibit ΣD^* values around 3, before the next points seemingly "jump" to $5.6 \leq \Sigma D^* \leq 6.0$. ΣD^* around the same region, where the biliquid nanofoam points of titration A2 are located. Since this region in the phase diagram is between the biliquid nanofoam regions formed along dilution lines A1 and A2, the biliquid nanofoam formed along dilution line B1 must also be O/W.

The dilution line of titration B3, starting from the binary mixture of 15 wt% surfactant and 85 wt% 2-ethylhexanol and extending towards the water corner of the phase diagram, only exhibits scattering with a pronounced broad peak due to the hydrogen-bonded alcohol network at high-q and a weak broad bump in the mid-q range due to random weak surfactant headgroup clusters, which also produce the low-q upturn, see Fig. 3. Almost all the surfactant is dissolved in the oil, which is also suggested by Teubner-Strey model fits to the mid-q range, see **Fig. S8**, and by a barely changing scattering invariant, see Fig. 4**B**. Shortly after w_{sat} is reached, there is macroscopic phase separation. No micro-emulsion phase is observed. The same is observed for titration B2 before the Onuki region is reached.

All Ornstein-Zernike + Broad Peak model fits of samples inside the biliquid nanofoam region, see Tables S13, S14, and S16, yield correlation lengths between 3.5 nm to 7.8 nm. The contributions of the Ornstein-Zernike term and the Broad Peak term to the fit is illustrated exemplary for sample B1-8 in the graphical abstract in lin-lin scale, in **Fig. S15A** in $\ln[(I(q)\text{-}background)\cdot q^2]$ versus q^2, and in **Fig. S15B** in log–log scale. The obtained average repeat distances, D*, corresponding to the average droplet, i.e., nanofoam cell, sizes are in a range of 10.6 nm to 32.2 nm. Wolf *et al.* [43–45] and Menold *et al.* [46,47] did not give systematic average sizes for their W/O biliquid nanofoams, but their cryogenic transmission electron microscope and freeze-fracture electron microscope images suggest cell sizes in the range of 20–50 nm. Thus, the average cell size of their W/O biliquid nanofoam is similar to the upper bound of the average cell size found in our O/W biliquid nanofoam ($\approx$ 30 nm). It is important to note that in the present system the thickness of the hydrophilic headgroup/water layer is expected to vary significantly depending on the number of water molecules available per headgroup. For a given constant number of water molecules per surfactant headgroup, the average cell size is found to increase with increasing oil content due to swelling of the hydrophobic interior. When adding water at a fixed oil to surfactant ratio, the average cell size also increases due to swelling of the hydrophilic bilayer with water. The order of magnitude of the number of 2-ethylhexanol per droplet is 10^2–10^4, a (significant) portion of which acts as a co-surfactant in the surfactant film. The calculation is given in **Note S4**. Since all water is bound as hydration water to the headgroups in the surfactant film, the water activity should be low.

It should also be noted that the impurities of the technical surfactant $C_8E_8CH_2COOH$ are not expected to significantly influence the reported phase behavior. Even after further purification by ion exchange, $C_8E_8CH_2COOH$ was generally found to behave similarly [7]. The only impurities that are potentially relevant to its phase behavior in the present system are the esters, see section 2.1., which are also involved in an auto-coacervation process observed at low surfactant concentrations in binary mixtures with water [2]. However, the small fraction of esters ($\leq$ 1.5 wt% of the surfactant) is not expected to change the reported phase behavior. Since the esters are more hydrophobic than the surfactant itself, the esters are expected to be dissolved in the oil-rich pseudo-phase first.

5. Conclusion and outlook

The main points established by measuring a large number of small-angle X-ray scattering data on absolute scale (some of them scatter 1000 times more than others), including the values of the scattering invariants, allow us to be certain that no O/W to W/O "inversion" occurs in this system with increasing oil content. At low water content, water hydrates the EO groups of $C_8E_8CH_2COOH$ molecules dissolved in 2-ethylhexanol and no commonly found reverse micelles are found. Moreover, when oil is added to an aqueous mixture of the surfactant, the curvature cannot reverse. Therefore, in the middle of the phase triangle, a nanometric biliquid foam exists. In this domain around 10^2–10^4 oil molecules form domains that are separated by hydrated headgroups forming polar lamellae.

The phase diagram shown in Fig. 2, can now be drawn with indications of the different structural regions, as shown in Fig. 9. There is no true structural inversion and the dehydrated (or only weakly hydrated) surfactant dissolves in the oil in the 2-ethylhexanol-rich corner. An interesting property of the observed biliquid nanofoam, schematically drawn in Fig. 9, is that it exists without any bulk water, with only water (weakly) bound to the surfactant headgroups. This means that the water activity is low, which might be of interest for certain chemical reactions, which could benefit from the oil-rich pseudo-phase as "nanoreactors" separated by a self-healing semi-permeable membrane.

To the best of our knowledge, this is also the first report of an O/W biliquid nanofoam, only W/O biliquid nanofoams having been reported so far [43–47]. In all these systems, e.g., in the water/NaCl – hexyl

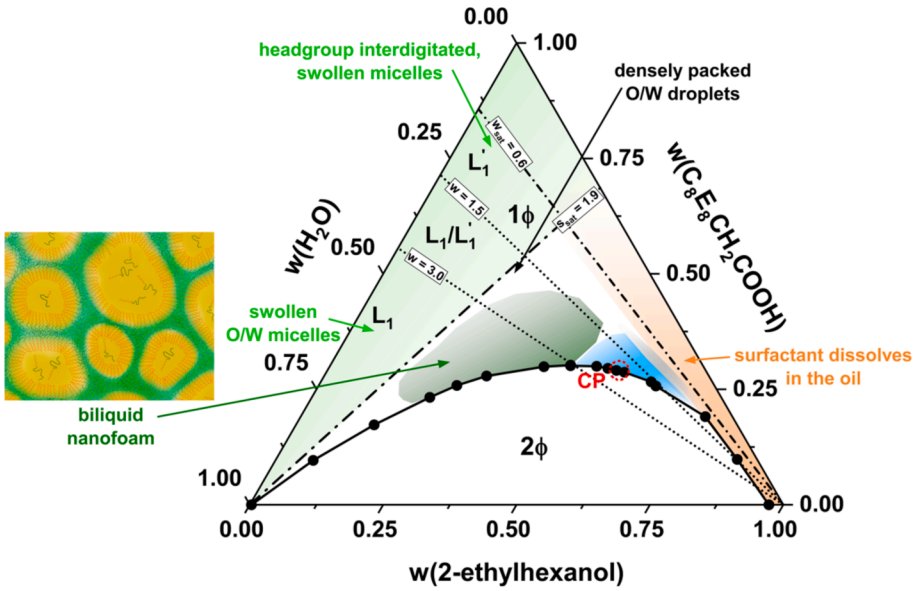

Fig. 9. Phase diagram of the ternary system 2-ethylhexanol – $C_8E_8CH_2COOH$ – H_2O with indications of the identified structures. Dash-dotted lines indicate the determined values of $w_{sat} = n_{sat}(H_2O)/n(EO)$ and $s_{sat} = n_{sat}(2\text{-ethylhexanol})/n(tail)$. The dotted lines at $w = 1.5$ and $w = 3.0$ indicate a region, where all water molecules are expected to be bound as hydration water for sure. L_1: Classical O/W (mixed) micelles. L_1': Direct micelles without free bulk water, when all water present is bound as hydration water. CP: Critical point. In the inset figure, the biliquid nanofoam is schematically drawn. Locally flat bilayers form hydrated surfactant headgroup layers (green), separating enclosed hydrophobic nanodroplets (yellow: 2-ethylhexanol-rich pseudo-phase; orange: surfactant tails). The surfactant molecules drawn inside the yellow domain represent the surfactant fraction dissolved in the hydrophobic nanodroplet. (For interpretation of the references to colour in this figure legend, the reader is referred to the web version of this article.)

methacrylate – dioctyl sulfosuccinate sodium salt (AOT) [46] system, the reverse biliquid nanofoam with droplet diameters of around 20–50 nm is formed by addition of small amounts of oil to the oil-free sponge phase (L_3). In our system, we have not observed a clear sign of a sponge phase, but a narrow transition via a sponge phase cannot be excluded, as the swelling plot also shows points around $\Sigma D^* = 3$, which could be a sponge phase but does not have to be. It rather seems that the biliquid nanofoam in the present system is achieved by actual "super-swelling" of direct micelles. To confirm this, additional experiments should be conducted in the future, especially conductivity and diffusion-order NMR spectroscopy could be helpful to determine if there are any transitions to bicontinuous states. Also, if a reverse biliquid foam was formed, the conductivity would be expected to be very low, as water-rich, ion containing droplets are separated by hydrophobic layers without charge carriers [46]. In our case, we therefore expect that there is no significant decrease of the conductivity when transitioning from the swollen micellar structure to the biliquid nanofoam structure. Another distinction to the biliquid nanofoam reported by Menold *et al.* [46,47] is that they observed a high viscosity in the biliquid nanofoam state, which we did not observe in our system. This could be due to the surfactant/co-surfactant films being much more flexible in our system compared to the double-chain AOT surfactant.

Another important aspect to note is that this biliquid nanofoam can only form because the oil acts as a co-surfactant to weaken the steric constraint of the very hydrophilic surfactant, which usually remains in spherical packing. If a purely hydrophobic oil, such as *n*-dodecane, is used, only a narrow swollen micellar region exists and if the micelles are fully loaded, a very *n*-dodecane-rich phase separates from the swollen micellar phase, see **Fig. S16**, which was semi-quantitatively shown using phase separation and physical density measurements. If one seeks to achieve a biliquid nanofoam in a system of a purely hydrophobic oil – $C_8E_8CH_2COOH$ – H_2O, one at least needs to add some co-surfactant to the system, otherwise the resistance to shape transitions of the surfactant is too strong.

Chemistry performed in the small "nano-reactors" made from about 10^2–10^4 oil/solvent molecules, separated by hydrophilic barriers of hydrated headgroups, should give original results, since the reacting molecules can be isolated. When needed, the sample could be heated shortly to 70–80 °C by microwave pulse for instance to dehydrate all headgroups, allowing easy collection by phase separation. Upon cooling again, the compartmentation of the sample is restored within seconds and a synthesis cycle can be restarted. If such an isolation is in fact possible for reactants, is still an open question that could be solved by spin-echo NMR, as first introduced by Peter Stilbs [56].

CRediT authorship contribution statement

Patrick Denk: Writing – original draft, Visualization, Validation, Methodology, Investigation, Formal analysis, Data curation, Conceptualization. **Selina Reigl:** Writing – review & editing, Investigation, Conceptualization. **Bastian Rödig:** Writing – review & editing, Investigation. **Michael Sztucki:** Validation, Supervision, Methodology, Data curation. **Sylvain Prévost:** Validation, Supervision, Methodology. **Thomas Zemb:** Writing – review & editing, Validation, Supervision, Methodology, Formal analysis, Conceptualization. **Werner Kunz:** Writing – review & editing, Validation, Supervision, Resources, Conceptualization.

Declaration of competing interest

The authors declare that they have no known competing financial interests or personal relationships that could have appeared to influence the work reported in this paper.

Acknowledgement

We acknowledge the European Synchrotron Radiation Facility (ESRF) for provision of synchrotron radiation facilities under proposal number SC-5453 (DOI: 10.15151/ESRF-ES-1438785010) and we would like to thank Theyencheri Narayanan and Laurent Jacqmin for assistance and support in using beamline ID02. We also thank Diego Pontoni for granting access to a PSCM laboratory. We are grateful to Thomas

Myrdek from Kao Chemicals GmbH for providing the surfactant free of charge and sharing useful information.

Appendix A. Supplementary data

Supplementary data to this article can be found online at https://doi.org/10.1016/j.jcis.2025.01.090.

Data availability

Data will be made available on request. SAXS data will be accessible at doi: 10.15151/ESRF-ES-1438785010.

References

[1] P. Denk, A. El Maangar, J. Lal, D. Kleber, T. Zemb, W. Kunz, Phase diagrams and microstructures of aqueous short alkyl chain polyethylene glycol ether carboxylate and carboxylic acid triblock surfactant solutions, J. Colloid Interface Sci. 590 (2021) 375–386, https://doi.org/10.1016/j.jcis.2021.01.061.

[2] P. Denk, A. El Maangar, S. Prévost, W. Silva, R. Gschwind, T. Zemb, W. Kunz, Cloud point, auto-coacervation, and nematic ordering of micelles formed by ethylene oxide containing carboxylate surfactants, J. Colloid Interface Sci. 621 (2022) 470–488, https://doi.org/10.1016/j.jcis.2022.04.046.

[3] O.G. Mouritsen, L.A. Bagatolli, LIFE - AS A MATTER OF FAT, Springer International Publishing, Cham (2016), https://doi.org/10.1007/978-3-319-22614-9.

[4] M. Rothe, E. Müller, P. Denk, W. Kunz, Ionic Liquids Based on the Concept of Melting Point Lowering Due to Ethoxylation, Molecules 26 (2021) 4034, https://doi.org/10.3390/molecules26134034.

[5] K. Lunkenheimer, S. Schrödle, W. Kunz, Dowanol DPnB in water as an example of a solvo-surfactant system: adsorption and foam properties, in: Trends in Colloid and Interface Science XVII, Springer, Berlin Heidelberg, Berlin, Heidelberg, 2004, pp. 14–20, https://doi.org/10.1007/b93970.

[6] S. Queste, P. Bauduin, D. Touraud, W. Kunz, J.-M. Aubry, Short chain glycerol 1-monoethers—a new class of green solvo-surfactants, Green Chem. 8 (2006) 822–830, https://doi.org/10.1039/B603973A.

[7] P. Denk, L. Matthews, S. Prévost, T. Zemb, W. Kunz, A dilute nematic gel produced by intramicellar segregation of two polyoxyethylene alkyl ether carboxylic acids, J. Colloid Interface Sci. 659 (2024) 833–848, https://doi.org/10.1016/j.jcis.2024.01.014.

[8] F. Cattelaens, M. Jäger, T. Myrdek, Purification of carboxymethylated fatty alcohol derivates using ion exchange resins, J. Surfactant Deterg. 26 (2023) 111–117, https://doi.org/10.1002/jsde.12641.

[9] T. Narayanan, M. Sztucki, T. Zinn, J. Kieffer, A. Homs-Puron, J. Gorini, P. Van Vaerenbergh, P. Boesecke, Performance of the time-resolved ultra-small-angle X-ray scattering beamline with the Extremely Brilliant Source, J. Appl. Cryst. 55 (2022) 98–111, https://doi.org/10.1107/S1600576721012693.

[10] M. Teubner, R. Strey, Origin of the scattering peak in microemulsions, J. Chem. Phys. 87 (1987) 3195–3200, https://doi.org/10.1063/1.453006.

[11] S. Prévost, M. Gradzielski, T. Zemb, Self-assembly, phase behaviour and structural behaviour as observed by scattering for classical and non-classical microemulsions, Adv. Colloid Interface Sci. 247 (2017) 374–396, https://doi.org/10.1016/j.cis.2017.07.022.

[12] S. Prévost, T. Zemb, Using Weak Aggregation for Solubilization and Separation, in: P. Lindner, J. Oberdisse (Eds.), Neutrons, X-Rays, and Light Scattering Methods Applied to Soft Condensed Matter, 2nd ed., Elsevier, 2024.

[13] S. Prevost, T. Lopian, M. Pleines, O. Diat, T. Zemb, Small-angle scattering and morphologies of ultra-flexible microemulsions, J. Appl. Cryst. 49 (2016) 2063–2072, https://doi.org/10.1107/S1600576716016150.

[14] L.S. Ornstein, F. Zernike, Accidental deviations of density and opalescence at the critical point of a single substance, Proc. Akad. Sci.(Amsterdam) XVII (1914) 793–806. http://www.dwc.knaw.nl/DL/publications/PU00012727.pdf.

[15] M. Gradzielski, M. Duvail, P.M. de Molina, M. Simon, Y. Talmon, T. Zemb, Using Microemulsions: Formulation Based on Knowledge of Their Mesostructure, Chem. Rev. 121 (2021) 5671–5740, https://doi.org/10.1021/acs.chemrev.0c00812.

[16] E. Pensini, A.G. Marangoni, B. Bartokova, A.L. Fameau, M.G. Corradini, J. A. Stobbs, Z. Arthur, S. Prévost, Sulfolane clustering in aqueous saline solutions, Phys. Fluids 36 (2024), https://doi.org/10.1063/5.0196389.

[17] S.M. Choi, S.H. Chen, T. Sottmann, R. Strey, The existence of three length scales and their relation to the interfacial curvatures in bicontinuous microemulsions, Physica A 304 (2002) 85–92, https://doi.org/10.1016/S0378-4371(01)00524-6.

[18] T.N. Zemb, I.S. Barnes, P.J. Derian, B.W. Ninham, Scattering as a critical test of microemulsion structural models, in: Trends in Colloid and Interface Science IV, Steinkopff, Darmstadt, 1990, pp. 20–29, https://doi.org/10.1007/BFb0115518.

[19] A. Onuki, Surface tension of electrolytes: Hydrophilic and hydrophobic ions near an interface, J. Chem. Phys. 128 (2008), https://doi.org/10.1063/1.2936992.

[20] A. Onuki, S. Yabunaka, T. Araki, R. Okamoto, Structure formation due to antagonistic salts, Curr Opin Colloid, Interface Sci. 22 (2016) 59–64, https://doi.org/10.1016/j.cocis.2016.02.007.

[21] R. Okamoto, A. Onuki, Theory of nonionic hydrophobic solutes in mixture solvent: Solvent-mediated interaction and solute-induced phase separation, J. Chem. Phys. 149 (2018) 19–27, https://doi.org/10.1063/1.5037673.

[22] L. Xu, P. Kumar, S.V. Buldyrev, S.-H. Chen, P.H. Poole, F. Sciortino, H.E. Stanley, Relation between the Widom line and the dynamic crossover in systems with a liquid–liquid phase transition, in: Proceedings of the National Academy of Sciences 102, 2005, pp. 16558–16562, https://doi.org/10.1073/pnas.0507870102.

[23] S. Schöttl, T. Lopian, S. Prévost, D. Touraud, I. Grillo, O. Diat, T. Zemb, D. Horinek, Combined molecular dynamics (MD) and small angle scattering (SAS) analysis of organization on a nanometer-scale in ternary solvent solutions containing a hydrotrope, J. Colloid Interface Sci. 540 (2019) 623–633, https://doi.org/10.1016/j.jcis.2019.01.037.

[24] S. Lüsse, K. Arnold, The interaction of poly(ethylene glycol) with water studied by 1H and 2H NMR relaxation time measurements, Macromolecules 29 (1996) 4251–4257, https://doi.org/10.1021/ma9508616.

[25] C. Branca, S. Magazù, G. Maisano, F. Migliardo, P. Migliardo, G. Romeo, Hydration Study of PEG/Water Mixtures by Quasi Elastic Light Scattering, Acoustic and Rheological Measurements, J. Phys. Chem. B 106 (2002) 10272–10276, https://doi.org/10.1021/jp014345v.

[26] P.G. Nilsson, B. Lindman, Water self-diffusion in nonionic surfactant solutions. Hydration and Obstruction Effects, J. Phys. Chem. 87 (1983) 4756–4761, https://doi.org/10.1021/j100246a041.

[27] O. Tirosh, Y. Barenholz, J. Katzhendler, A. Priev, Hydration of polyethylene glycol-grafted liposomes, Biophys. J . 74 (1998) 1371–1379, https://doi.org/10.1016/S0006-3495(98)77849-X.

[28] A. Patra, A. Bandyopadhyay, S. Roy, J.A. Mondal, Origin of Strong Hydrogen Bonding and Preferred Orientation of Water at Uncharged Polyethylene Glycol Polymer/Water Interface, J. Phys. Chem. Lett. 14 (2023) 11359–11366, https://doi.org/10.1021/acs.jpclett.3c03098.

[29] J.-F. Dufrêche, T. Zemb, Bending: from thin interfaces to molecular films in microemulsions, Curr. Opin. Colloid Interface Sci. (2020), https://doi.org/10.1016/j.cocis.2020.06.001.

[30] P. Lindner, J. Oberdisse (Eds.), Neutrons, X-Rays, and Light: Scattering Methods Applied to Soft Condensed Matter, 2nd ed., Elsevier, 2024 https://shop.elsevier.com/books/neutrons-x-rays-and-light/lindner/978-0-443-29116-6.

[31] G. Porod, General theory, in: O. Glatter, O. Kratky (Eds.), Small Angle X-Ray Scattering, Academic Press Inc., New York, 1982, pp. 17–51.

[32] R.F. Schmidt, S. Prévost, M. Gradzielski, T. Zemb, Structure of microemulsions in the continuous phase channel, The European Physical Journal E 46 (2023) 76, https://doi.org/10.1140/epje/s10189-023-00337-z.

[33] S.H. Chen, E.Y. Sheu, J. Kalus, H. Hoffman, Small-angle neutron scattering investigation of correlations in charged macromolecular and supramolecular solutions, J. Appl. Cryst. 21 (1988) 751–769, https://doi.org/10.1107/S0021889888008052.

[34] O. Abillon, B.P. Binks, C. Otero, D. Langevin, R. Ober, Winsor microemulsions with cationic surfactants: structure, J. Phys. Chem. 92 (1988) 4411–4416, https://doi.org/10.1021/j100326a033.

[35] J. Jouffroy, P. Levinson, P.G. de Gennes, Phase equilibria involving microemulsions (Remarks on the Talmon-Prager model), J. Phys. 43 (1982) 1241–1248, https://doi.org/10.1051/jphys:019820043080124100.

[36] Y. Talmon, S. Prager, Statistical thermodynamics of phase equilibria in microemulsions, J. Chem. Phys. 69 (1978) 2984–2991, https://doi.org/10.1063/1.437016.

[37] T.N. Zemb, S.T. Hyde, P.J. Derian, I.S. Barnes, B.W. Ninham, Microstructure from x-ray scattering: the disordered open connected model of microemulsions, J. Phys. Chem. 91 (1987) 3814–3820, https://doi.org/10.1021/j100298a018.

[38] P. Denk, Packing Constraint of Octaoxyethylene Octyl Ether Carboxylates in Micelles and Bicelles and Fibrillar Self-Assembly of Glycyrrhizic Acid Ammonium Salt, Dissertation, University of Regensburg (2024), https://doi.org/10.5283/epub.59263.

[39] M. Li, Y. Wakata, H. Zeng, C. Sun, On the thermal response of multiscale nanodomains formed in trans-anethol/ethanol/water surfactant-free microemulsion, J. Colloid Interface Sci. 652 (2023) 1944–1953, https://doi.org/10.1016/j.jcis.2023.08.166.

[40] M. Li, L. Yi, C. Sun, Spontaneously formed multiscale nano-domains in monophasic region of ternary solution, J. Colloid Interface Sci. 628 (2022) 223–235, https://doi.org/10.1016/j.jcis.2022.07.152.

[41] K. Sadakane, H. Seto, Membrane Formation in Liquids by Adding an Antagonistic Salt, Front. Phys. 6 (2018) 1–11, https://doi.org/10.3389/fphy.2018.00026.

[42] T.N. Zemb, The DOC model of microemulsions: microstructure, scattering, conductivity and phase limits imposed by sterical constraints, Colloids Surf A Physicochem Eng Asp 129–130 (1997) 435–454, https://doi.org/10.1016/S0927-7757(97)00061-7.

[43] L. Wolf, H. Hoffmann, Y. Talmon, T. Teshigawara, K. Watanabe, Cryo-TEM imaging of a novel microemulsion system of silicone oil with an anionic/nonionic surfactant mixture, Soft Matter 6 (2010) 5367, https://doi.org/10.1039/c0sm00049c.

[44] L. Wolf, H. Hoffmann, K. Watanabe, T. Okamoto, Microemulsions from silicone oil with an anionic/nonionic surfactant mixture, PCCP 13 (2011) 3248, https://doi.org/10.1039/c0cp00062k.

[45] H. Hoffmann, Structure formation in surfactant solutions, Adv. Colloid Interface Sci. 178 (2012) 21–33, https://doi.org/10.1016/j.cis.2012.06.001.

[46] P. Menold, R. Strey, U. Olsson, Z. Takacs, D. Topgaard, C. Stubenrauch, Transition from a sponge-like to a foam-like nanostructure in a water-rich L3 phase: A confirmation, Colloids Surf A Physicochem Eng Asp 705 (2025) 135747, https://doi.org/10.1016/j.colsurfa.2024.135747.

[47] P. Menold, R. Strey, S. Roitsch, N. Preisig, C. Stubenrauch, Transition from a Sponge-Like to an Onion-Like Nanostructure in the L3 Phase – Part I, J. Colloid Interface Sci. 653 (2024) 1743–1752, https://doi.org/10.1016/j.jcis.2023.09.194.

[48] S.J. Chen, D.F. Evans, B.W. Ninham, Properties and structure of three-component ionic microemulsions, J. Phys. Chem. 88 (1984) 1631–1634, https://doi.org/10.1021/j150652a038.
[49] D.F. Evans, D.J. Mitchell, B.W. Ninham, Oil, water, and surfactant: properties and conjectured structure of simple microemulsions, J. Phys. Chem. 90 (1986) 2817–2825, https://doi.org/10.1021/j100404a009.
[50] K.J. Lissant, The geometry of high-internal-phase-ratio emulsions, J. Colloid Interface Sci. 22 (1966) 462–468, https://doi.org/10.1016/0021-9797(66)90091-9.
[51] K.J. Lissant (Ed.), Emulsions and Emulsion Technology: Part I, Marcel Dekker Inc, New York, 1974.
[52] I.S. Barnes, S.T. Hyde, B.W. Ninham, P.J. Derian, M. Drifford, T.N. Zemb, Small-angle x-ray scattering from ternary microemulsions determines microstructure, J. Phys. Chem. 92 (1988) 2286–2293, https://doi.org/10.1021/j100319a038.
[53] I.S. Barnes, P.-J. Derian, S.T. Hyde, B.W. Ninham, T.N. Zemb, A disordered lamellar structure in the isotropic phase of a ternary double-chain surfactant system, J. Phys. 51 (1990) 2605–2628, https://doi.org/10.1051/jphys:0199000510220260500.
[54] D. Roux, C. Coulon, M.E. Cates, Sponge phases in surfactant solutions, J. Phys. Chem. 96 (1992) 4174–4187, https://doi.org/10.1021/j100190a017.
[55] O. Sonneville-Aubrun, V. Bergeron, T. Gulik-Krzywicki, B. Jönsson, H. Wennerström, P. Lindner, B. Cabane, Surfactant Films in Biliquid Foams, Langmuir 16 (2000) 1566–1579, https://doi.org/10.1021/la990599k.
[56] P. Stilbs, Fourier transform pulsed-gradient spin-echo studies of molecular diffusion, Prog Nucl Magn Reson, Spectrosc 19 (1987) 1–45, https://doi.org/10.1016/0079-6565(87)80007-9.